POLITECNICO DI MILANO

Facoltà di Ingegneria Industriale

Corso di Laurea Magistrale in Ingegneria Meccanica

FEM analysis of spider web inspired structures

Relatore: Prof. Marco Virginio Boniardi
Co-relatore: Prof. Frédérick Gosselin

Tesi di Laurea di:
Luca Berto
Matricola 766666

Anno Accademico 2012 – 2013

POLITECNICO DI MILANO

POLYTECHNIQUE MONTRÉAL

FEM analysis of spider web inspired structures

Luca Berto

Maîtrise cours en génie mécanique

Laboratoire de mécanique multi-échelles (LM2)

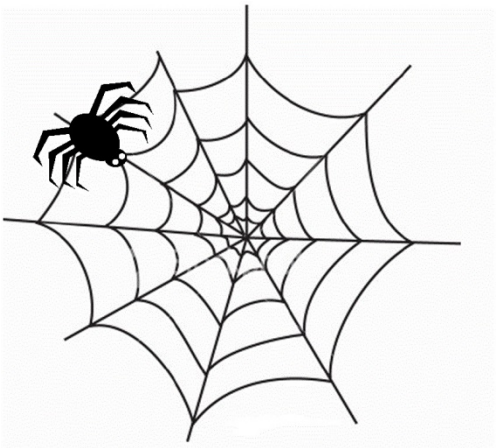

Director: Frédérick Gosselin Co-Director: Daniel Therriault

May 2013

Alla mia famiglia.
Grazie per il vostro sostegno.

Ringraziamenti

Grazie ai miei genitori che mi hanno sempre supportato e sopportato nella mia vita. Mi avete sempre dato nuovo entusiasmo e aiutato a realizzare i miei obiettivi e i miei sogni.

Grazie alle mie sorelle che mi hanno accompagnato e dato un riferimento crescendo assieme in famiglia. Grazie per tutte le volte che mi avete spinto a provare nuove avventure.

Grazie agli amici e compagni di università, in Italia e no, che mi hanno spesso aiutato nei modi più vari per arrivare fino a qui.

Infine un ringraziamento anche a coloro che hanno contribuito alla mia formazione dandomi l'opportunità di fare esperienza e il potenziale per le realizzazioni future.

Remerciements

Je souhaite remercier Frédérick Gosselin et Daniel Therriault pour l'opportunité de développer ce projet chez le Laboratoire de mécanique multi-échelles (LM2).

Mon directeur de stage Frédérick Gosselin pour les précieux indications et conseils pendant mon travail. Je me rappellerai de ton attitude gentille et ta capacité de proposer toujours de nouvelles idées pour guider mon parcours.

Le travail a été facilité par l'atmosphère amicale qui règne au laboratoire LM2 et par la disponibilité de tous à aider les autres. Je tiens à remercier particulièrement Nicolas Guerin, Maxime Arguin, Benjamin LeDafniet, Renaud Passieux et Xavier Cauchy pour toutes les journées passé ensemble à travaille et à rire.

Je pense à tous les amis pour votre aide pendant les cours et la vie à Montréal.

Je veux aussi remercier toutes les personnes de l'école polytechnique de Montréal qui m'ont donné leur temps et ont eu la patience de m'aider

Contents

Riassunto

Questa ricerca è nata dall'idea di riprodurre in laboratorio le caratteristiche meccaniche della seta di ragno e la struttura della ragnatela con materiale plastico. Lo scopo è di creare una struttura capace di resistere all'impatto di un oggetto utilizzando una minima quantità di materiale. Lo studio è costituito da due parti: una sperimentale nella quale si spiega la produzione dei filamenti, le prove eseguite e l'analisi dei risultati dei test; un'altra in cui si utilizzano gli esiti precedenti per sviluppare un modello a elementi finiti (FEM) per studiare il comportamento della struttura ragnatela.

Una ragnatela (Figure 1-1) è il risultato dell'evoluzione naturale di una struttura il cui scopo è procurare cibo intercettando insetti volanti quindi l'analogia è evidente. Inoltre, dovendo il ragno sintetizzare la seta, la quantità di materia utilizzata è ottimizzata per ridurre il consumo energetico avere quindi un bilancio favorevole tra l'energia richiesta per la creazione della ragnatela e quella ricavata dalle prede.[1]

La seta di ragno è un materiale particolarmente interessante per le sue proprietà: i ragni sono in grado di produrne sette tipologie differenti ognuna con una specifica funzione [6]. Nelle ragnatele sono due i tipi di seta presenti. Il telaio esterno e i raggi sono fatti di seta proveniente della ghiandola Major Ampullate (MA), più rigida, mentre la spirale di cattura è costituita da seta viscida, più deformabile. Entrambe hanno una tenacità superiore ai materiali ingegneristici dovuta alla loro capacità di deformazione elevata (Table 1-1), anche la capacità di dissipare energia per isteresi (65%) è una proprietà importante. La disposizione dei fili di sete diverse nella ragnatela è strettamente legato alla capacità della stessa di resistere ai sovraccarichi ed eventualmente subire cedimenti solamente locali [11 e 12]. Infatti, lo sforzo dovuto al carico esterno si distribuisce sul 30% del materiale vicino al punto d'impatto quando vi è deformazione plastica. La stessa disposizione geometrica non garantisce uguali risultati se al posto della seta di ragno si utilizzano altri materiali (Figure 1-5).

Da un'analisi delle proteine che costituiscono la seta di ragno si evidenzia che sono presenti dei legami sacrificali che nascondono una parte della molecola al carico. La rottura di queste giunzioni permette alla struttura di dissipare energia, grazie allo stiramento della parte di proteine ripiegate su se stesse, e incrementando la lunghezza sottoposta al carico creando così una deformazione maggiore (Figure 1-6 - Figure 1-8).

Approccio sperimentale

I filamenti sono stati prodotti tramite la tecnica di scrittura diretta utilizzando un robot cartesiano equipaggiato con una siringa e una centralina di controllo della pressione nel pistone che regola il flusso in uscita dalla siringa (Figure 2-1). La siringa era riempita con una soluzione al 25% di PLA in peso disciolto nel DCM (vedere paragrafo 2.1.1 Solution preparation). Il processo di direct writing prevede la deposizione della soluzione su un substrato e regolando i parametri seguenti diverse tipologie di filo possono essere ottenute (Figura i).

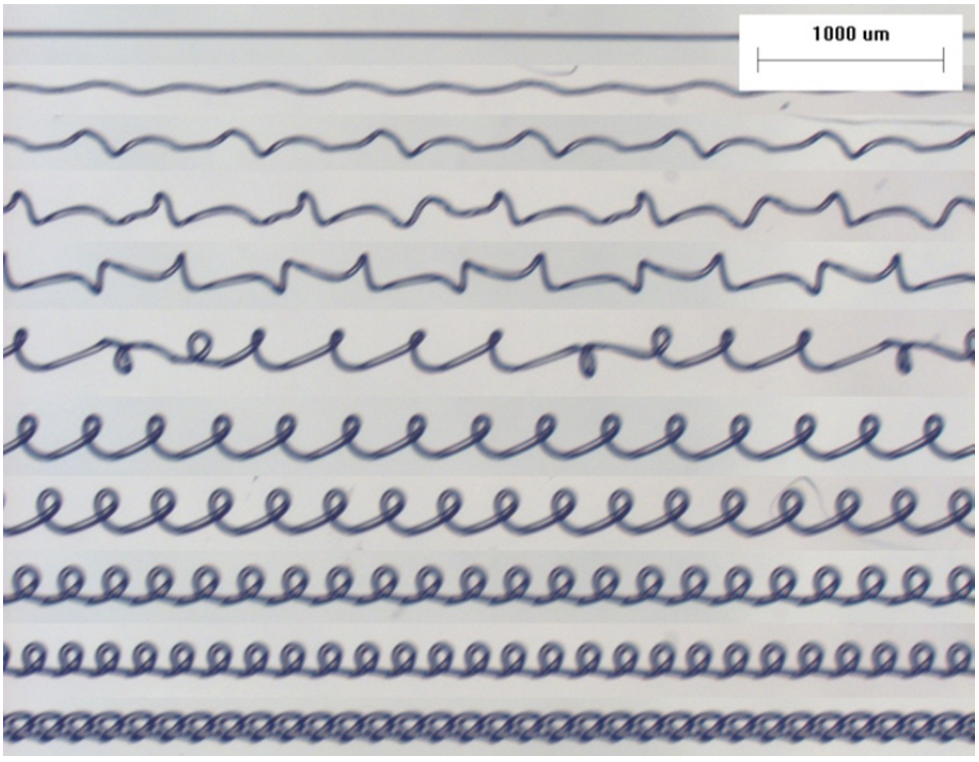

Figura i Sequenza di fili realizzati da Frédérick Gosselin con un ago di 30µm di diametro, 300µm di altezza e velocità del substrato di 2 mm/s. La velocità del flusso aumenta dall'alto verso il basso.

I parametri sono (Figura ii) :

- La velocità relativa tra substrato e flusso della soluzione
- La pressione nella siringa cioè la velocità di uscita della soluzione
- L'altezza dell'ago rispetto al substrato

La velocità relativa substrato-flusso è la composizione della velocità di uscita della soluzione dall'ago della siringa, regolata dalla pressione, e della velocità relativa traslatoria tra siringa e substrato. Regolando i parametri di deposizione le diverse tipologie di fili possono essere prodotte, in particolare per ottenere l'instabilità viscosa desiderata. Grazie a questo fenomeno d'instabilità un liquido viscoso, ad esempio il miele o lo sciampo, che è colato su una superficie piana può creare degli anelli. Se aggiungiamo una velocità relativa tra la superficie e la sorgente del liquido, gli anelli si disporranno uno a fianco dell'altro creando così una catena di unioni sacrificali (Figure 1-10). Nel caso di creazione dei legami sacrificali la deposizione deve esser tale da permettere la fusione dei due tratti quando il filamento si sovrappone per chiudere l'anello: questo implica che la velocità di formazione degli anelli e quella di evaporazione del DCM dalla soluzione sono legate tra loro. Trovare il buon rapporto tra le due per ottenere delle giunzioni resistenti che si rompano prima del cedimento del filo non è facile, soprattutto se si cerca una ripetibilità dei risultati. Questo aspetto è ancora da risolvere.

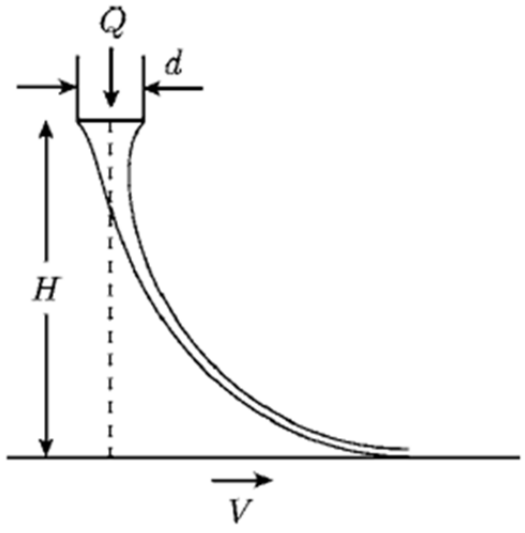

Figura ii Schema del flusso in uscita dalla siringa.

Una volta prodotta una serie di fili questi venivano osservati al microscopio in cerca di difetti evidenti e ne veniva misurato il diametro tramite un software di analisi delle immagini.

L'ultima fase del lavoro sui fili era la prova meccanica di trazione effettuata grazie a una cella di carico da 5N e con una velocità di deformazione di 0.01 [mm/mm/s]. I dati così ottenuti venivano poi analizzati ed elaborati prima di esser impiegati nelle simulazioni FEM.

I fili per i quali sono stati ottenuti dei risultati affidabili nei test meccanici erano dei fili rettilinei, senza giunzioni sacrificali, prodotti con i parametri riportati in (Table 2-1). I dati evidenziano tre distinte fasi ad andamento lineare nella curva forza-spostamento che si ritrovano anche nella curva sforzo-deformazione (Figure 2-9 e Figura iii). La prima fase è caratterizzata da una rigidezza elevata seguita poi da un plateau in cui lo sforzo quasi non varia nonostante l'ampia deformazione. Nell'ultima fase il materiale si irrigidisce nuovamente fino ad arrivare a rottura. È importante notare che la definizione di deformazione usata non è la classica di Cauchy ma quella di Hencky che prevede il logaritmo del rapporto tra lunghezza attuale e iniziale eq.(a). Una volta ottenute le curve di sforzo-deformazione al fine di poter utilizzare i dati nel calcolo a elementi finiti si è applicato un modello di interpolazione lineare per trovare una curva rappresentativa media a tratti. Quest'ultima è stata validata confrontando la sua energia di rottura con quella delle curve sperimentali.

$$\varepsilon_H = \int_{L_0}^{l} \frac{\delta l}{l} = \ln\left(\frac{l}{L_0}\right) \qquad \text{(a)}$$

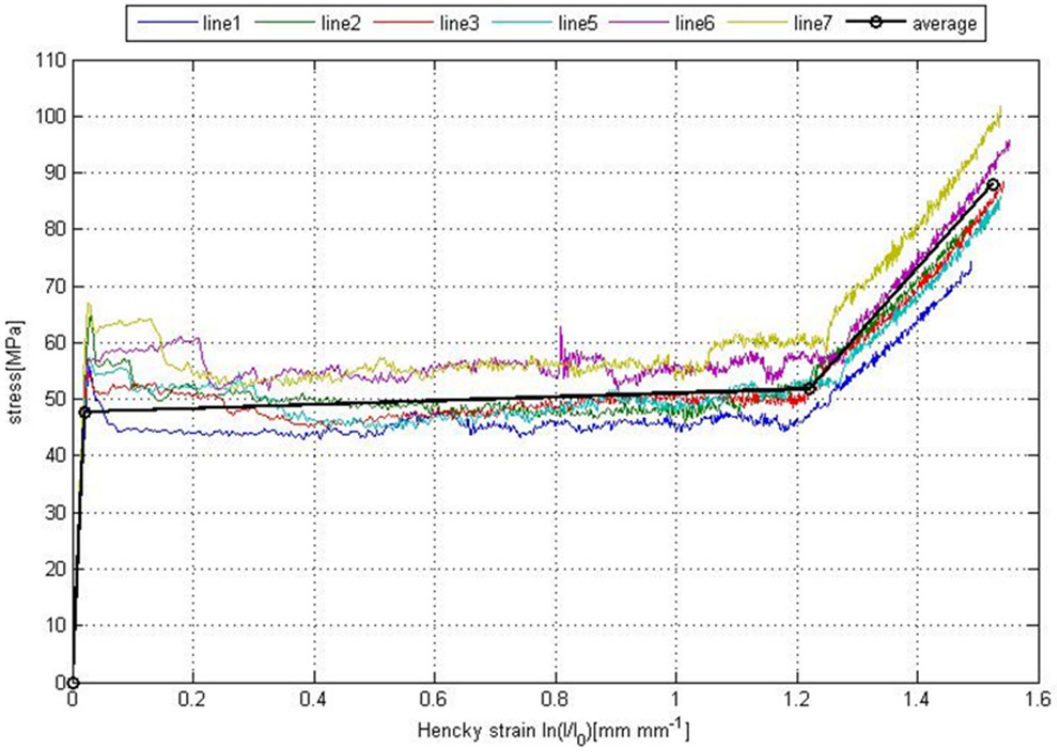

Figura iii Andamento sforzo-deformazioni delle prove di trazione e curva media.

Modelli a elementi finiti

Per passare dal singolo filo alla ragnatela uno studio FEM era necessario per comprendere il comportamento meccanico e la funzione delle varie componenti. Questa analisi è stata effettuata utilizzando il software ANSYS e degli elementi di tipo Truss che considerano solamente la componente assiale di sforzo, come avviene in un filo. La curva caratteristica del materiale ricavata in precedenza è stata utilizzata per i casi di materiale multilineare mentre un modello lineare avente uguali condizioni di rottura, sforzo e deformazione (Figure 3-1), è stato usato come caso di confronto per evidenziare l'influenza del materiale. La modellazione FEM ha tenuto quindi conto di due non linearità: una dovuta alle grandi deformazioni sempre presente e l'altra alla caratteristica del materiale, quest'ultima solo nel caso di materiale multilineare. I limiti delle simulazioni sono stati imposti per conservare l'integrità della struttura, il corpo esterno che impatta sulla ragnatela non deve attraversarla. Si è imposta la deformazione massima del materiale per evitarne la rottura quindi con considerazioni geometriche si è

ricavato il massimo spostamento fuori piano ammissibile e il numero necessario di raggi nella ragnatela (3.1Structural design). Si è scelto di imporre la deformazione del materiale invece dello spostamento trasversale finale della struttura per poter sfruttare tutte le proprietà del materiale.

Si è scelto di affrontare prima due casi semplici in cui un solo filo è sottoposto al carico trasversale: in un primo momento il carico è applicato in mezzaria del filo e successivamente viene decentrato a un quarto della lunghezza totale (Figure 3-2 e Figure 3-5). In entrambi i casi una soluzione analitica delle equazioni di equilibrio è stata trovata ed è stata confrontata con le soluzioni dei vari casi di carico simulati agli elementi finiti con ottima corrispondenza dei risultati sia per il materiale lineare che multilineare. Nel caso di carico centrato si riscontra un miglior comportamento del materiale multilineare per spostamenti trasversali minori: è richiesta una forza maggiore rispetto al materiale lineare per ottenere lo stesso affondamento. Nel caso di carico decentrato il materiale multilineare è migliore in quanto richiede sempre una forza più elevata.

Successivamente altre due geometrie sono state analizzate:

- sola struttura radiale
- la ragnatela completa, cioè è stata aggiunta la spirale alla struttura radiale (spirale e raggi dello stesso materiale)

anche per questi casi si sono studiati la differenti combinazioni di carico centrato e decentrato con le caratteristiche del materiale. Nel caso di carico centrato ritroviamo lo stesso comportamento visto in precedenza quindi si può concludere che la spirale non ha effetto (Figura iv). Se il carico è decentrato invece la spirale aumenta notevolmente la resistenza della struttura (Figura v) anche considerando solamente il materiale lineare con un numero di raggi inferiore.

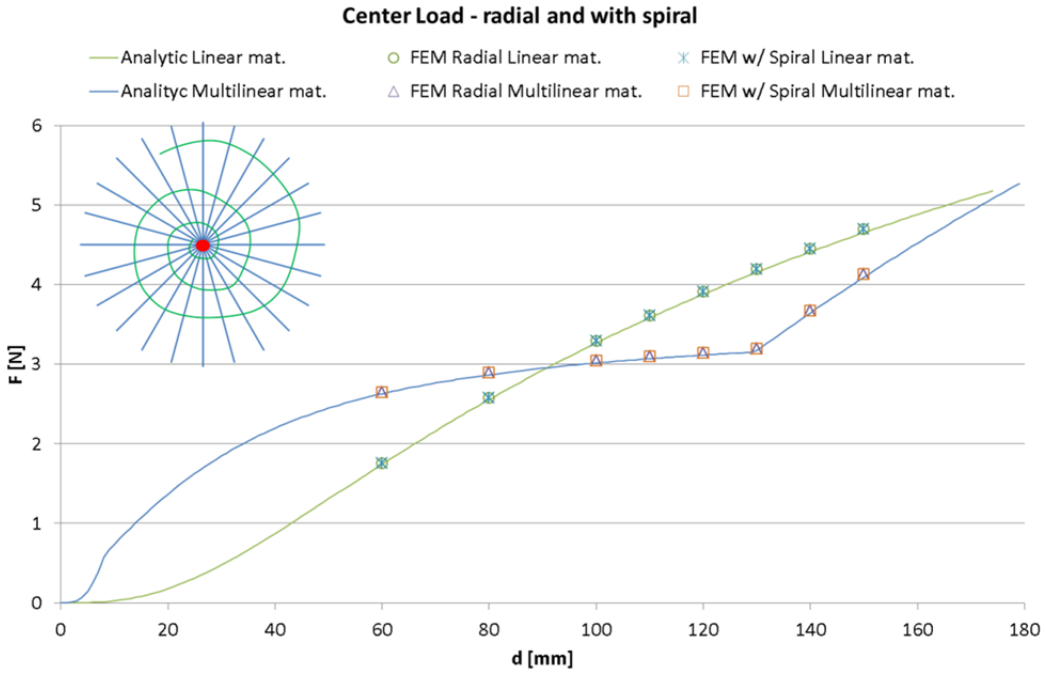

Figura iv Carico centrato. Struttura solo radiale e completa.

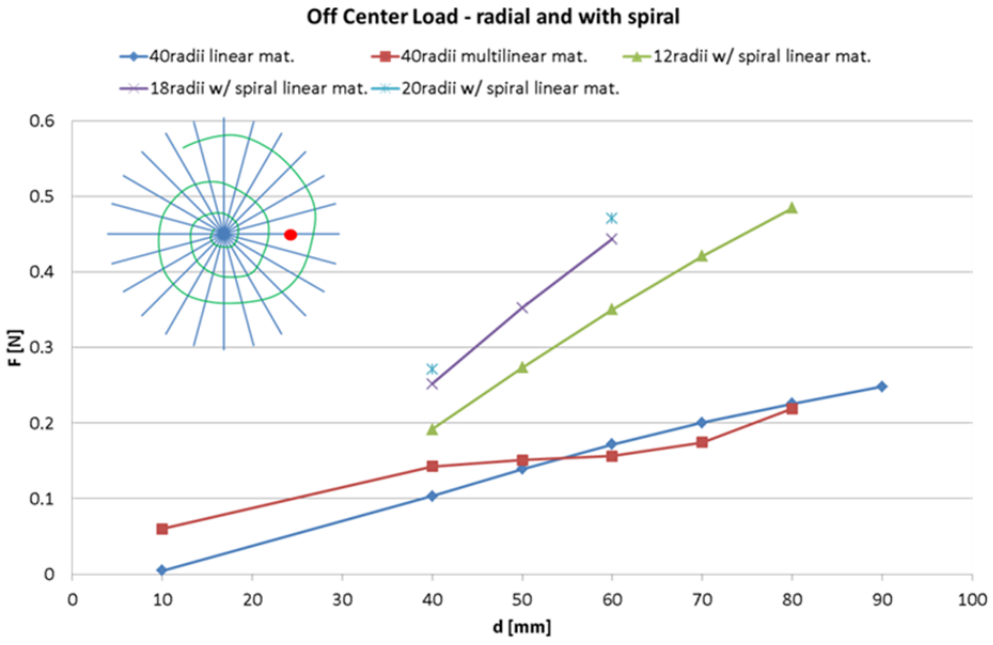

Figura v Carico decentrato. Importanza della spirale.

Conclusioni e lavori futuri

Il progetto inizialmente era molto ampio e sebbene non si sia arrivati sin dove si voleva molto è stato fatto e, almeno per i fili dritti, dei test di impatto sono prossimi a venire. Un metodo di lavoro completo e dettagliato nelle varie fasi è stato sviluppato e potrà essere utilizzato anche su nuovi studi, ad esempio con legami sacrificali.

Le simulazioni FEM hanno prodotto buoni risultati da validare con ulteriori esperienze di laboratorio. Si è ritrovato il comportamento previsto dalla letteratura infatti anche per il materiale utilizzato la zona in cui gli sforzi raggiungono la plasticizzazione resta limitata ai dintorni del punto in cui il carico è applicato mentre il resto della struttura rimane in regime elastico. Come già detto, l'importanza della spirale è evidente se il carico non è perfettamente centrato mentre il materiale multilineare è superiore poiché richiede una forza maggiore a pari spostamento trasversale.

Dei miglioramenti sono possibili specie nella produzione del fili: studiare di più l'influenza dei parametri per ottenere risultati ripetibili. Altre prove meccaniche vanno realizzate idealmente prima dei test di impatto come la trazione con velocità di deformazione più elevata oppure per validare sperimentalmente i risultati FEM si potrebbe testare un filo con carico trasversale. Per quanto riguarda la simulazione a elementi finiti nuove geometrie, come ad esempio altre tipologie di spirale o dei cerchi concentrici, potrebbero essere interessanti da paragonare. Una miglioria importante sarebbe trovare un metodo che permetta di calcolare, almeno indicativamente, il numero di iterazioni per risolvere una simulazione.

Abstract

The capability of a spider web structure to absorb energy by deforming itself without breaking is like no other structure in the world. The structure light weight and its capability to trap a flying prey are the result of natural evolution thus now we try to learn from spiders how to build a more efficient structure to absorb kinetic energy.

In this project both the material and the structure are studied and tried to be reproduced with polymeric material (PLA). First a literature review is done in the introduction then the production and testing of PLA thread is described. FEM simulations are developed to analyze different structural elements functions and behavior according to material's properties. The results demonstrate that the spiral in an orb-web structure is important when the external load is applied off center on the web and that a linear material is not good in this application.

A complete approach is developed to put together the experimental and simulation aspects. The procedure and tools used here can easily be readapted to further studies.

Keywords: spider web, spider silk, impact energy, non-linear simulation, viscous instability

Chapter 1. Introduction

The impact of an object on a structure is a really prohibitive load situation. The structure has to absorb the kinetic energy and dissipate it somehow without allowing to the object going through the structure. This is the idea behind a bullet-resistant vest or a containing cell for an aircraft engine; they are designed to save lives by preventing a bullet or a turbine blade perforating them. A way to obtain the required protection is using a material able to absorb much energy without failing, for instance with a high deformation capability.

As often happen, it is possible to find similar phenomena in the natural world thus we can be inspired by them and try to copy the operating principle. Very interesting is the particular system that has been developed by spiders. The spider's webs are structures that have attracted many scientific studies with their complexity and their properties. When we think of a spider's web we normally are considering an orb web (Figure 1-1) that is specifically made to trap a flying prey, an insect, thus the comparison with intercepting structures is evident. Moreover, these natural artifacts have an incredible material weight to energy dissipation ratio, i.e. interception capability.

A spider orb web is a complicated system based on interaction of different aspects: from the macroscopic geometry and the mechanical material's properties to the microscopic chemical production process with internal protein structure of the silk. The mechanical aspect is the one that will be considered here: the geometry as inspiration and the properties as goal. There will be also a connection to the behavior of particular internal silk's structures whose toughness is increased in an interesting way. In fact a mechanism to increment the deformation of a filament is creating sacrificial bonds that allow to add some hidden length to the filament without increasing his apparent initial length thus gaining deformation and so toughness.

1.1 Spider orb-web and silk

Orb-webs are a perfect example of optimization in nature. Their structure consists in different parts that work all together to capture the prey. An orb-web is a planar net which works like a filter to catch the insects. Threads are organized in order to reach the largest area to intercept the prey undergoing the constraint of a finite available volume of material. The web geometry of different spider species is always similar in spite of the myriad of possible solutions, this means that the evolution has led to a single optimal solution: an overall planar structure able to provide food at the minimum cost for the spider. The synthesis of silk is very costly and using a limited volume reduces the ratio between the energy expenditure and that gained as food from preys [1].

[2] has studied the geometry of spider webs and their construction procedure by spiders: they have several radii (approximately each ten degree) connected with an Archimedean spiral and a central hub where the spider can feel every vibration from anywhere in the web [1]. Other studies on web's geometry have been done highlighting the non-symmetrical structure to compensate: gravity, to facilitate the movement of the spider and the prey capture. [3] studied the effect of environmental condition on the geometry and strength of orb-webs. The surrounding structures and thus the area to cover with the web has a double influence on the geometry: for instance in a rectangular frame the spider uses less radii and places them in order to cover the longer side; because the volume of silk that can be produced by a spider, the larger is the frame the less is the capture area occupied by the spiral and the mesh becomes wide especially with consecutive orb-weaving, i.e. from the third web. Indeed the time elapsed between successive webs is related with web size. External factors have an influence on web and silk properties, for instance if the web is built in windy conditions its dimension is smaller than in still air but the resistance when a weight is applied is higher, i.e. it sags less. Orb-web structure is affected also by the kind of prey to capture and the size and weight of the spider [4] in fact a bigger spider, who eats bigger preys therefore needs a tougher structure, builds smaller but asymmetric webs. Asymmetry brings to a non-uniform load distribution thus internal tension in web's threads particularly in upper radii [5].

Spider silk is a specialized material that has mechanical properties comparable to or even higher than manmade materials: metals and best synthetic fibers. There are seven different types of silks that are produced by spiders' glands (Figure 1-2), each having different properties and being used to accomplish different functions; their properties change based on the spinning conditions, environmental humidity, temperature and also internal status to the spider, and manipulation after the synthesis, like immersion in water that leads to plasticization, [6] [7] [8]. Silk proteins have been identified and patented but no human production similar to this material has succeeded yet, thus natural silks are used in many fields from medicine to fabrics. Spiders have developed many types of silk according to specific functions, more than other insects, thus each one is highly specialized and their study can provide important information.

Most of actual knowledge is related to two different kinds of silk, those by which an orb web is made: the major ampullate (MA) silk and the viscid silk. The major ampullate gland produces the silk used for the web frame, this is the radii and the external structure, and is also used as spider's draglines, the fibers which the spider uses to lower itself. The viscid silk is produced by the flagelliform (FL) gland and constitutes the web's spiral, the structure in charge of trapping the insect [9]. The viscid silk has to provide the deceleration to stop the prey without breaking but also has to dissipate the kinetic energy thus not to act like an elastic and catapult it back whence it came and has to grab the insect till the spider comes to eat it, for this reason it is covered by a sticky layer. The organization is illustrated in (Figure 1-3). For these two silk types mechanical tensile data are available since much research has been done, and thus a comparison with other materials is possible (Table 1-1). Considering synthetics materials like Kevlar, carbon fiber and high-tensile steel, MA has a lower stiffness of more than one order of magnitude and a lower strength, even though of the same order of magnitude and very similar to the high-tensile steel one. This makes the engineering materials better to support the load and transmit the force, indeed they are designed for it. Therefor the real distinguishing factor is in the extensibility of spider's silks, both MA and viscid, associated to their toughness. Only rubber has a better deformability and a similar, but lower, value of toughness. On the other hand synthetic rubber has many magnitudes less in Young modulus and breaking

stress. Thus those mechanical properties make breaking these natural materials a high energy consuming process.

Figure 1-1A spider's orb web (taken from http://www.dangeroustime.com/2013/01/a-spiders-web-covered-in-ice.html)

Table 1-1 Tensile mechanical properties of spider silks and other materials (taken from [9]).

Material	Stiffness, E_{init} (GPa)	Strength, σ_{max} (GPa)	Extensibility, ε_{max}	Toughness (MJ m^{-3})	Hysteresis (%)
Araneus MA silk	10	1.1	0.27	160	65
Araneus viscid silk	0.003	0.5	2.7	150	65
Bombyx mori cocoon silk	7	0.6	0.18	70	
Tendon collagen	1.5	0.15	0.12	7.5	7
Bone	20	0.16	0.03	4	
Wool, 100 % RH	0.5	0.2	0.5	60	
Elastin	0.001	0.002	1.5	2	10
Resilin	0.002	0.003	1.9	4	6
Synthetic rubber	0.001	0.05	8.5	100	
Nylon fibre	5	0.95	0.18	80	
Kevlar 49 fibre	130	3.6	0.027	50	
Carbon fibre	300	4	0.013	25	
High-tensile steel	200	1.5	0.008	6	

The data for *Araneus* silks are from Denny (1976) and our laboratory. Other data have been taken from Wainwright et al. (1982), Gordon (1978, 1988) and Vincent (1982), without specific references because they are intended to indicate the relative magnitude rather than exact values.

MA silk, silk from the major ampullate gland; RH, relative humidity.

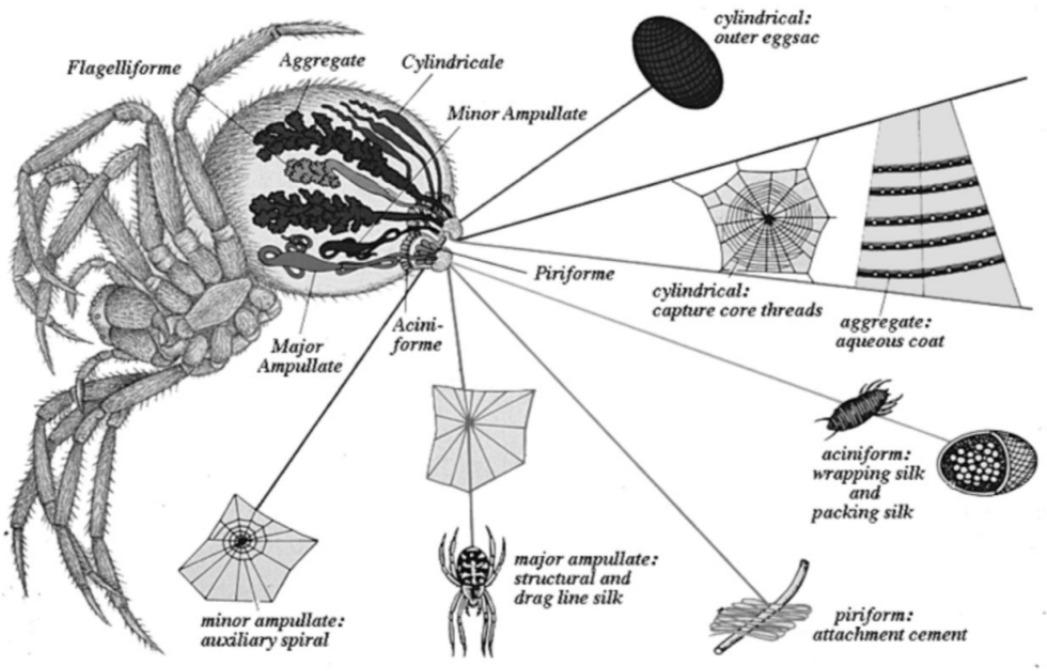

Figure 1-2 Spider's anatomy: glands ant threads (taken from [6]).

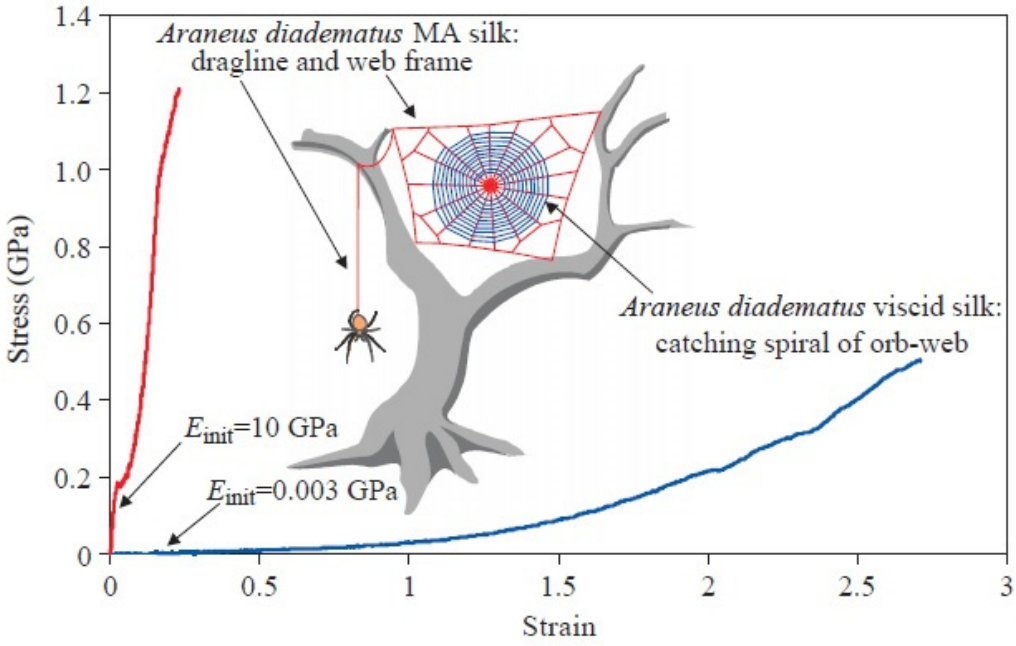

Figure 1-3 Spider web structure and silk properties: MA silk in red and viscid silk in blue. E_{init} is the initial stiffness. (taken from [9]).

The silk properties are optimized for their particular application in the web. The viscid silk has a deformation capability ten times greater than the MA silk and a Young modulus three orders of magnitude lower. That's because its function is to intercept the prey and it does not have a structural role. Compared with other materials in the table the viscid silk's strain is similar to biomaterials like elastin and resilin but it is lower than the synthetic rubber. This high extensibility is the aspect to be recreated in this study.

The previous analysis was based on tension tests but the real operational conditions for spider silk are normally caused by a perpendicular loading. They have to capture a flying prey thus its kinetic energy has to be dissipated somehow and not only stored and then released back to the prey like a spring catapult. The energy is absorbed by the material toughness and the hysteresis cycle of the silk, over 65% of the energy is lost in internal friction as heat, (see Figure 1-4 left). This high dissipating behavior allows the spider's orb web to be light because only a reduced volume of silk is necessary to trap the prey and thus reduced energy consumption for the spider to produce the silk. Fibers can be of 1 micron or so in diameter [10] and sometimes more than just one is used to achieve the required strength, creating a strand. Non-orb-weaver spiders, like the black widow, use a 3D web where the silk does not need to be so strong because energy is dissipated just by breaking some threads. All these properties are function of the strain rate as for viscoelastic materials and become more consistent with higher deformation velocity as happen in a prey impact on the orb web (Figure 1-4 right).

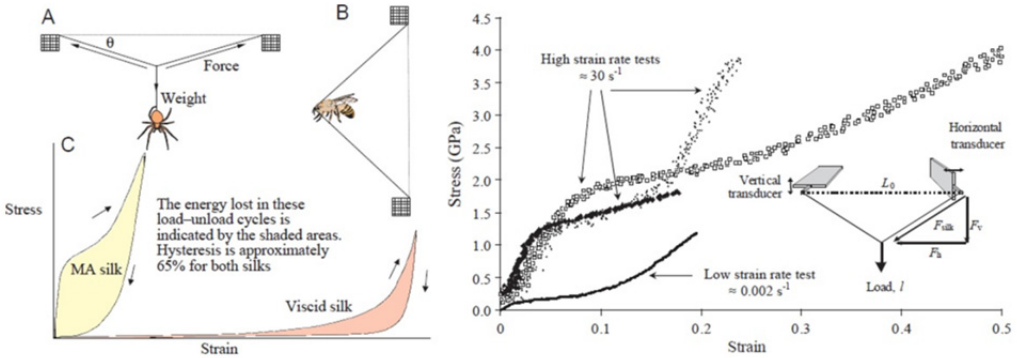

Figure 1-4 Left: real loading conditions of MA silk (A) and viscid silk (B) with a representation of the hysteresis cycles (C). Right: the effect of strain rate on mechanical MA silk's properties with a scheme of the measurement set-up (taken from [9]).

Energy absorption in an orb web could be thought to be associated to different factors as the aerodynamic drag, since the web covered area is important, or the internal repartition between the radial and spiral threads. A study on how the kinetic energy is dissipated [11] illustrates the different contribution of spiral and radial silks, the aerodynamic dissipation (drag) and the possible influence of web's geometry.

Spider's silks have an important damping capacity, the hysteresis of the material, that adsorbs the kinetic energy of the prey converting it into heat through the molecular friction. In [11] the authors have studied different spider webs undergoing simulated prey impacts and the larger contribution was always given by radial threads, up to 90% of the initial energy. Even when the simulated prey passed through the web breaking some threads, the reduction of its kinetic energy was proportional to the number of broken radii and no influence of the spiral components or the drag was found. Moreover, is important to remark how the geometry of the web allows the repartition of the load on different threads. This stress distribution depends on the prey's energy. It becomes concentrated in a local area when the initial kinetic energy increases, mainly because the higher is the kinetic energy the less is the time available for stress propagation. The quick load transfer combined with the material behavior produce a local high stress so a limited damage, when the prey passes through. The larger part of the energy is always dissipated by approximately 30% of the silk volume in the web, which reaches plastic stress, while the rest of the material volume takes part to the dissipation with only the elastic deformation. This suggests that spiders have built a structure able to maintain its functionality by breaking locally instead of undergoing to a global failure thus a damage tolerant structure.

A study of how different materials' behaviors influence the effects that a local or global, i.e. wind, load has on orb web geometry was made in [12]. Based on finite elements simulations and experiments, the analysis of the behavior of an orb web structure undergoing a targeted load was developed. Using different materials' models (linear, elastic-perfectly plastic and nonlinear representing the dragline behavior) as threads' property in the orb web geometry, the damage produced by the load applied on a spiral thread or on a radial one was studied, until structure break was reached. The web deformation is bigger when the force is on a radius than on a spiral thread but in both cases the damage always affects only a small

region near the radius of load application or a single thread in the spiral filament loaded case. However the charge does not yields the structure to the overall failure (Figure 1-5 a and b). Moreover, a web with defects can have a higher final load capacity this meaning that the structure is designed to work precisely even if it has lost its integrity (Figure 1-5 c). The spider's silk is the material that produces the best results thank to its softening behavior after the yield point which ensure that many radii participate to load resistance but only the one where the charge is applied can reach the third and final stiffening part of the curve till the breaking point. Thus the web structure has the capability to tolerate the presence of damages and to undergo local failures when overloaded. The structure design and behavior are justified also if the spider metabolism is considered indeed it has to repair only a small sector instead of rebuild the whole structure, being the silk spinning a high consuming energy process [13].

1.2 Hidden length and sacrificial bonds

Molecular analyses have led to the identification in structural molecules, composites [14], spider capture viscid silk [15] and biomaterials [16] of a mechanism to enhance the fracture toughness, i.e. energy dissipation: sacrificial bonds. A sacrificial bond is an internal connection in the molecule structure that breaks before the main structural link because they are weaker. This mechanism is coupled with a hidden length, which can be represented as a loop for a filament binds to itself, that is constrained from stretching because the load flows through the bond bypassing the hidden length. So when the bond breaks an additional segment of the molecule, which was not loaded before, appears and is unrolled. The total fiber's length grows, the force applied decreases almost to zero after the break then unrolling the new segment and stretching it makes the load increase again till the break of the next sacrificial bond, in a repetitive looped fiber, or the break of the main structure (Figure 1-6). The total energy required to break the molecule, the area under the curve, is increased by the breaking of the bond, first peak, and the additional red area to unroll and stretch the hidden length.

Appling many times this mechanism it is possible to obtain a sequence of peaks corresponding to each sacrificial bond, obtaining a saw-teeth profile in a tension result curve with load drops and rises following to the breaking and unrolling of a bond. In theory, for a

single strand with a parallel working bonds structure, the breaking force should increase, or at least be the same, with the filament stretch because the first bond to break is the weaker (Figure 1-7). Many combinations are possible as illustrated in [14] and all have a characteristic behavior. The toughness of the material increases as the energy to break the structure is used first to break the bonds and then to stretch the hidden length.

Sacrificial bonds are used in natural systems as in manmade artifact: in [16] is shown that bones have similar processes when fracture occurs; spider capture silk has internal bonds that keep the proteins compact when relaxed and are self-healing (Figure 1-8) also in rock fall protecting meshes this mechanism is used [17] (Figure 1-9).

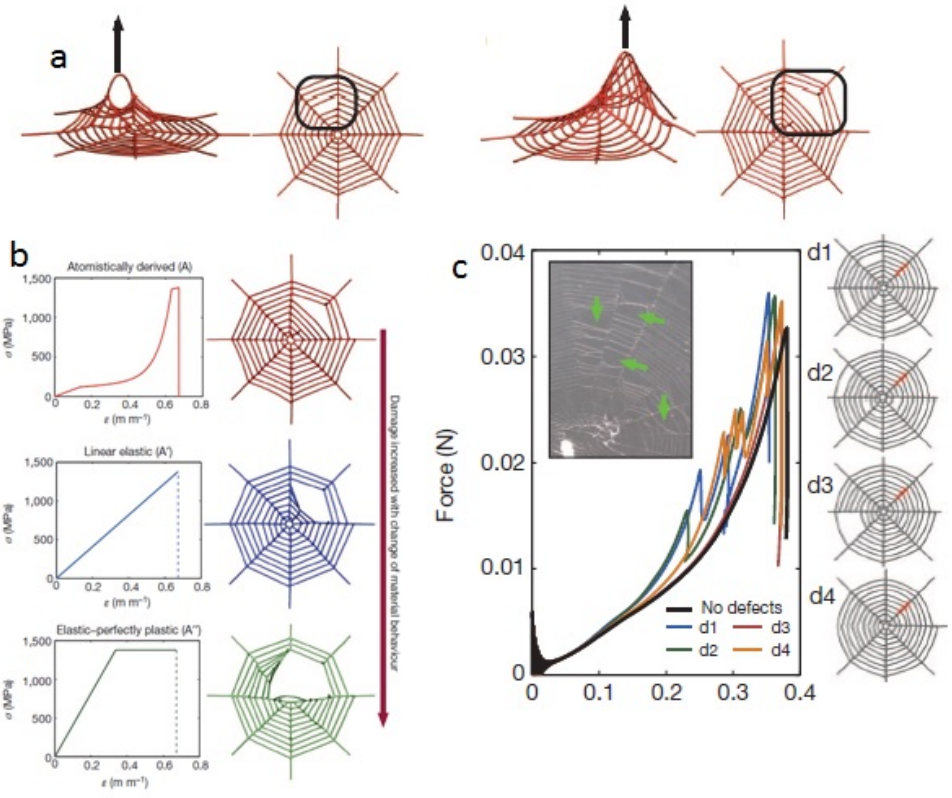

Figure 1-5 a) load on different threads: spiral (left) radial (right); b) spiral sector failure under radial loading for different material models and c) web defect (or occurred damage) tolerance (taken from [12])

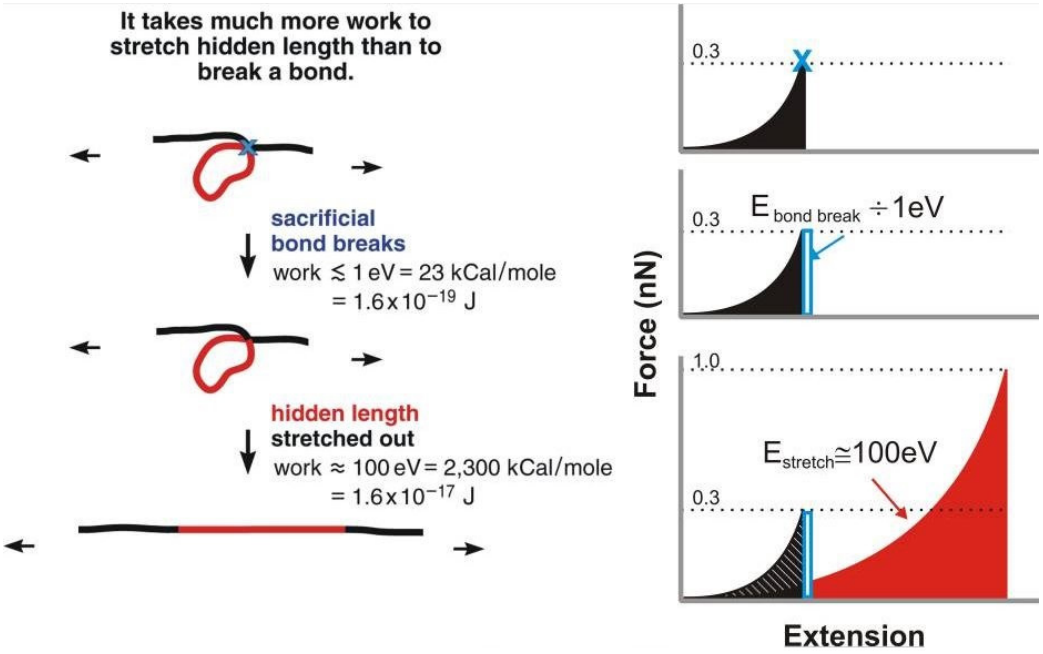

Figure 1-6 Sacrificial bond and hidden length mechanism: at the beginning only the black part is loaded, reached the breaking force of the bond the hidden length in red is stretched and the whole length (red plus black) contributes till the final structure break (taken from [14]).

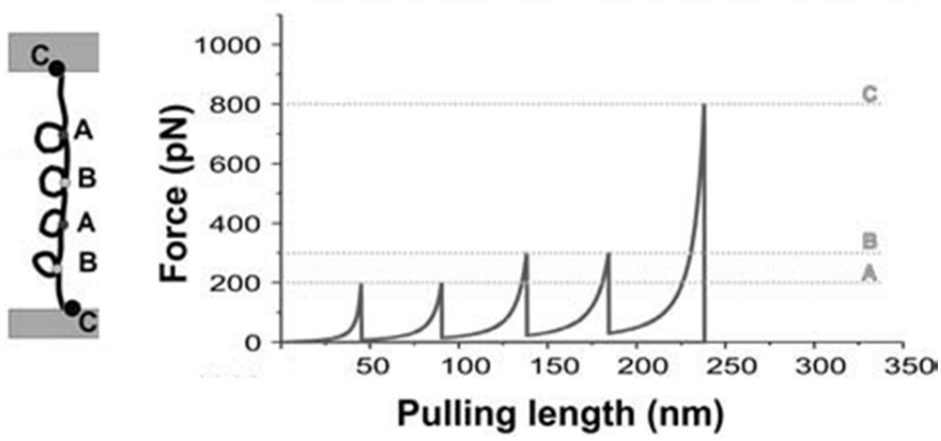

Figure 1-7 Single strand with parallel working sacrificial bonds and resulting tension test behavior: stretching the thread the bonds break according to their strength (taken from [14]).

Figure 1-8 Molecular models for relaxed and extended flagelliform protein sequences from spider capture silk (viscid silk) (taken from [15]).

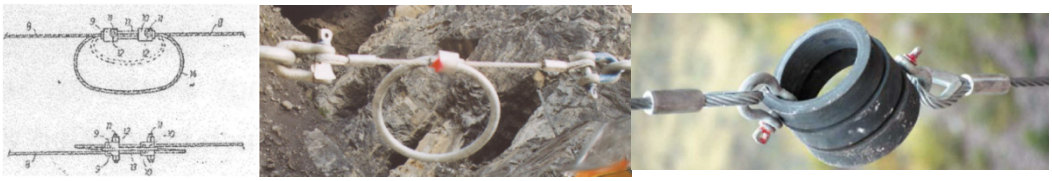

Figure 1-9 Types of absorption elements in rock fall protection meshes: hidden length with friction between ropes (left), bent steel pipe circle narrowing under tension (center) and elongating spiral spring (right) (taken from [17]).

1.3 Application in the study

The aim is to create a material with elevated toughness like spider's silk and using structures similar to the orb-web to intercept an object, ideally preventing it from breaking through or at least reducing significantly its residual energy. The approach was inspired by sacrificial bonds. The idea was to have a fiber with two different dimensions: a macroscopic structure of a thread and on a microscopic scale a thread coiled up in a sequence of loops. The obtained fiber could be considered as a strand whose properties are determined by its microscopic geometry, geometry which is designed during the fabrication process. This way instead of relying only on the properties of the material, by which the fiber is made, it is possible to add a microscopic improvement so that the global behavior will result in an enhanced final toughness.

To obtain this double nature a new production approach was used: starting from a limited volume of liquid solution the design of the fiber is made. The control on what could be called the internal geometry of the thread is given by the phenomenon of the instability in a viscous liquid when it is poured on a surface. This instability is produced by the interaction of the gravitational and viscous forces. When the instability is established the fluid filament starts to bend and creates repetitive circles [18]. It is possible to observe this phenomenon in a variety of common situation when a liquid like honey or shampoo is poured on a horizontal plane from a specific height.

If between the substrate and the fluid source there is no relative speed the result will be that the circles pile themselves in a coil (Figure 1-10 left) but if a linear relative velocity exists the circles will be aligned one aside the other. The latter is the approach used in this project to obtain a fiber with a sequence of loop (Figure 1-10 center and right). The point where the loop close on itself creates the sacrificial bond, because there is a solid junction, hiding all the circle length until it breaks.

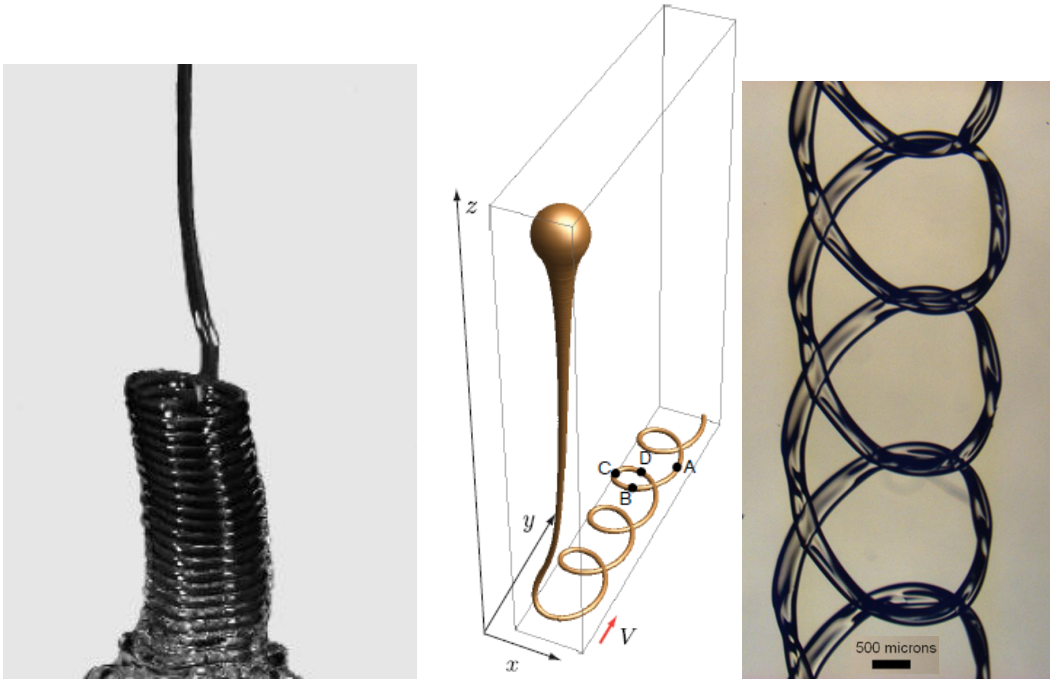

Figure 1-10 Left: example of viscid instability on fixed substrate that produces a coil. Center: viscous instability representation. Right: example of wire realized with a 200μm diameter of the needle.

Chapter 2. Experimental approach

In this chapter the experimental features will be described and analyzed: from the threads production to the tests results and data analysis. This was a crucial part in the study because it is the connection with the reality, to obtain the desired fiber thus not only having a theoretic study. It is the most complicated aspect because of the difficulties to obtain the desired fiber, a well working type, repeatable and reliable, with suitable properties, elevated deformability and toughness. The steps are described in the order followed during experiments in the laboratory.

The experimental goal was to produce a wire typology which production was repeatable and with satisfactory mechanical properties.

2.1 Production procedure

The production is a very complex and demanding stage because the control and understanding of many parameters are required. These parameters are the liquid solution properties and the deposition variables that influence the viscous instability. Depending on the parameters and what was the production also the time factor was important, for example the 18cm web produced (Figure 5-1) took about 7 hours. A first study on the relation between different fiber typologies and deposition parameters was already made, [19], but it was focused on the $200\mu m$ needle which turned out not to be a good solution when tested under uniaxial tension. Despite the good deposition repeatability, mechanical properties prove to be unusable (see Chapter 4 Conclusions for more information).

2.1.1 Solution preparation

The polymer used in these experiments was the Polylactic acid or polylactide (PLA), which is a biodegradable polymer. It was labeled as PLA4032D and was provided by the École Polytechnique's chemical department on May 9 2012.

The experiments were realized with solutions of PLA and DCM[1] as solvent. Each solution was prepared at 25% in weight of PLA and was then leaved to rest for at least 3 days to obtain a homogeneous solution. To have a feedback on the solution percentage the empty bottle was weighed at the beginning, then the PLA, in solid spherical shape, was added using a precision scale and the necessary volume of DCM was calculated with its density :$\rho_{DCM} = 1.325\ [g/cm^3]$.

$$V_{DCM} = W_{PLA}\frac{3}{\rho_{DCM}}$$

Where W_{PLA} is the weight of PLA and V_{DCM} is the required volume of DCM to have a nominal 25% weight solution. Once the bottle was filled with solution's components it was weighed again thus to check the real solution weight percentage. The real value was calculated by:

$$W_{sol}^{r} = \left(W_{bottle\ after} - W_{bottle\ before}\right)$$

$$R_{PLA}^{w} = \frac{W_{PLA}}{W_{sol}^{r}}$$

Where W_{sol}^{r} is the real solution's weight and R_{PLA}^{w} is the real solution's components ratio.

2.1.2 Deposition procedure

The deposition process was based on micro fabrication by direct writing with a Cartesian precision robot (I&j2200-4) with four degrees of freedom (DOF), in addition to the three linear movement a rotation around the vertical axe was possible (Figure 2-1 and Figure 2-2). The robot repeatability for the translation axes is given by the manufacturer: $\pm 0.01\ mm$. The thread is deposited by a syringe, fixed on the robot, on a microscope slide used as substrate. The robot's DOF used are the three Cartesian components. The needle can move in the vertical direction z and on one of the two planar components (the y in the robot coordinates system) while the other planar coordinate (x) is associated with the substrate platform. The

[1] Dichloromethane (DCM) or methylene chloride has the ability to dissolve the PLA and its high volatility at room conditions ensure the solidification of the solution once exposed to the air in a short period of time.

movement of the robot is governed by a computer. In these experiments the rotation around the z axe was not used.

At least two-thirds of 5cc syringe volume was filled with the solution before the deposition trying not to have air bubble inside the liquid, to reduce their presence while pouring the solution from the bottle the syringe was gently turned. Later a better solution, tried in others experiments, was adopted: in a bottle cap two holes were drilled, the bigger one for the liquid flow and the smaller to let air enter the bottle while pouring. The syringe closed with a cap and a plastic piston head cover was left on a table for about three minutes, the time to prepare the instrumentation, with the needle end up in order to let the few air bubbles arrive closer to the exit. This way they would spill at first and would not remain inside the wire when it is extruded. Once the instrumentation was ready, the syringe was positioned in its support on the robot and the piston actuator was placed on top ready for the deposition.

The deposition's parameters are (Figure 2-3):

- The jet-substrate relative speed
- The pressure therefore the solution velocity at the needle
- The needle's height, this is the vertical distance from the substrate

The jet-substrate relative velocity is the composition of the substrate relative speed, i.e. needle's speed and substrate's, and the jet extrusion velocity, the solution speed at the needle. To regulate the pressure a pressure control unit was used (Figure 2-1) with a HP7 piston, which multiplies by seven the value indicated by the control unit. All pressure parameter values are indicated as the control unit value since it is the one on which a user has the control. The distance between the needle tip and the substrate is normally around ten times the needle diameter. To verify the height and to prevent breaking the needle, especially with the 30μm glass ones, a high resolution camera was placed on the edge of the robot thus to see the distance of some microns as order of magnitude. The camera was also useful during deposition giving the operator the possibility to check if the deposition was looking good. Modifying the parameters' values the type of wire obtained varies from a straight line to a squiggly line up to a looped line, close rings sequence, created by the instability effect of the flow (Figure 2-4).

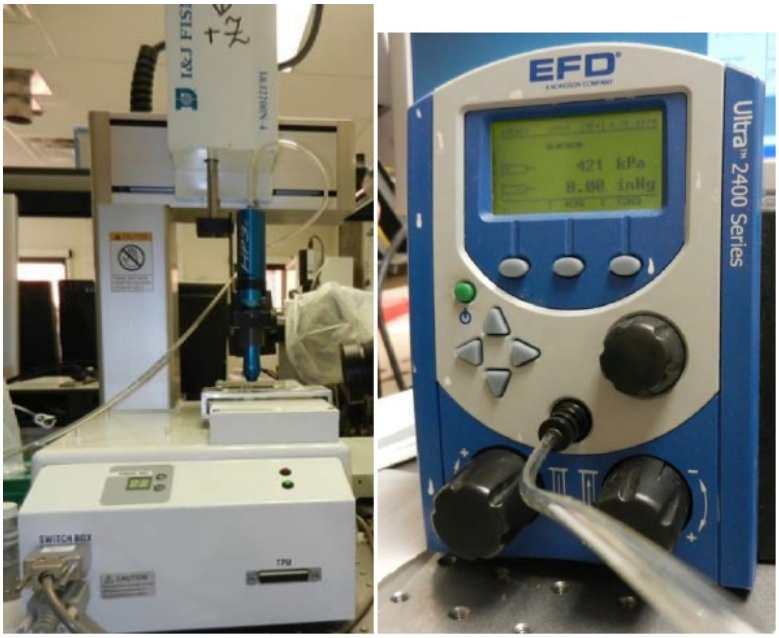

Figure 2-1On the left the deposition robot and on the right the pressure control unit.

Figure 2-2 Complite deposition station with the robot, the pressure control unit and the high resolution camera

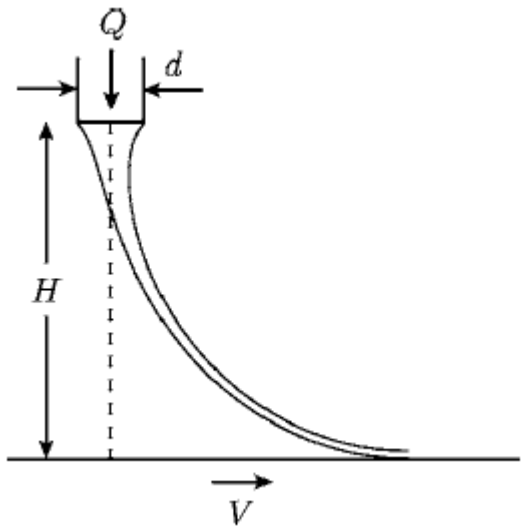

Figure 2-3Schematic representation of the deposition parameters: Q is the solution flow, d the needle diameter, H the height of the needle tip and V the relative speed of the needle and substrate.

The fabrication process begins and the liquid solution in the syringe is extruded on the substrate; the DCM evaporation through the section of the fiber transforms it into a quasi-dry solution. The evaporation time and jet velocity ratio characterized the strength of the links of the loops, they are the sacrificial bonds, thus is important to find the appropriate parameters.

The mechanical tests which were satisfactory were taken on a sequence of straight threads made with the following parameters:

Table 2-1 Deposition parameters

Pressure [KPa] (at control unit)	Substrate Speed [mm/s]	Height [mm]	Needle diameter [μm]
37	2	0.3	30

The needle used was a glass needle with an internal diameter of 30μm with a manufacturer declared variability of 20%. This range affects the deposition parameters so that each time the user has to make some adjustments. This is an important limitation for the production reproducibility and the development of a database with different parameters for each fiber type. During the deposition a pressure oscillation of $\pm 1 KPa$ was observed, and the height of

deposition was adjusted to compensate the non-perfect level of the microscope slide on the robot substrate.

2.1.3 Remarks

The operator has the direct control of three parameters: pressure, height of deposition and substrate speed. Jet velocity depends on pressure and could be calculated a priori with the Ostwald model, knowing the fluid properties and the needle diameter, or for a looped wire it can be inferred a posteriori evaluating the loops' periodicity, i.e. counting the number of loops per distance unit and their length to approximate the jet velocity as was done by [19]. With a jet velocity on substrate velocity ratio greater than one the thread will exhibit squiggly and the more the ratio increases the more the filament will present loops created by the instability phenomenon. The height of deposition is important to establish the instability and it modifies the loops' dimension and bond resistance, together with the jet velocity. The strength to break the sacrificial connections depends on the DCM evaporation during the deposition: a lower jet velocity and a greater deposition height increase the evaporation time available before the new filament coming out of the needle touches the other part of the thread already on the microscope slide, resulting in a less resistant junction or even in the absence of connection creating only an overlap. A fiber with overlaps should behave like a spring and could be interesting to analyze. On the other hand a higher jet speed will cause a fiber section deformation when the liquid flow touches the substrate resulting in a larger non circular section.

2.2 Measures

After at least one day that the threads were exposed to room conditions, to be sure of the complete evaporation of the DCM and solidification of the PLA even tough half a day is plenty enough, the picture of fibers were taken. The measures of threads' diameters were made with different microscope's lenses to observe the presence of defects or irregularities. This allowed also to remark the geometry of the filament: the loops' shape, dimension and eventual overlapping, or for straight threads the possible tension accumulated during deposition. Indeed if the substrate velocity is higher than the jet velocity the resulting fiber will be tensioned during the deposition so the fiber will be thinner. The thread's diameter was estimated with a 20x plus 0.5x zoom, after calibration, using the feature of the

software Image-pro plus 7.0 (by Media Cybernetics). The measures were made at least in three different points and then averaged to obtain the mean value which was considered as the effective diameter of the thread. In the whole study the fibers' sections were considered as perfectly circular that is an acceptable approximation for threads realized with smaller needles. An example of the measures is shown in Figure 2-5.

The results for the series are reported in Table 2-2, they are the mean values with the standard deviation.

Table 2-2 Measured diameters with standard deviation.

wire	mean Diameter [μm]	STD [μm]
line1	49.5828	1.1686
line2	45.9360	0.4679
line3	46.0870	0.2537
line4	43.1974	0.6341
line5	46.0860	0.5292
line6	43.8731	0.3213
line7	41.8256	0.4582
average	45.2268	0.5476

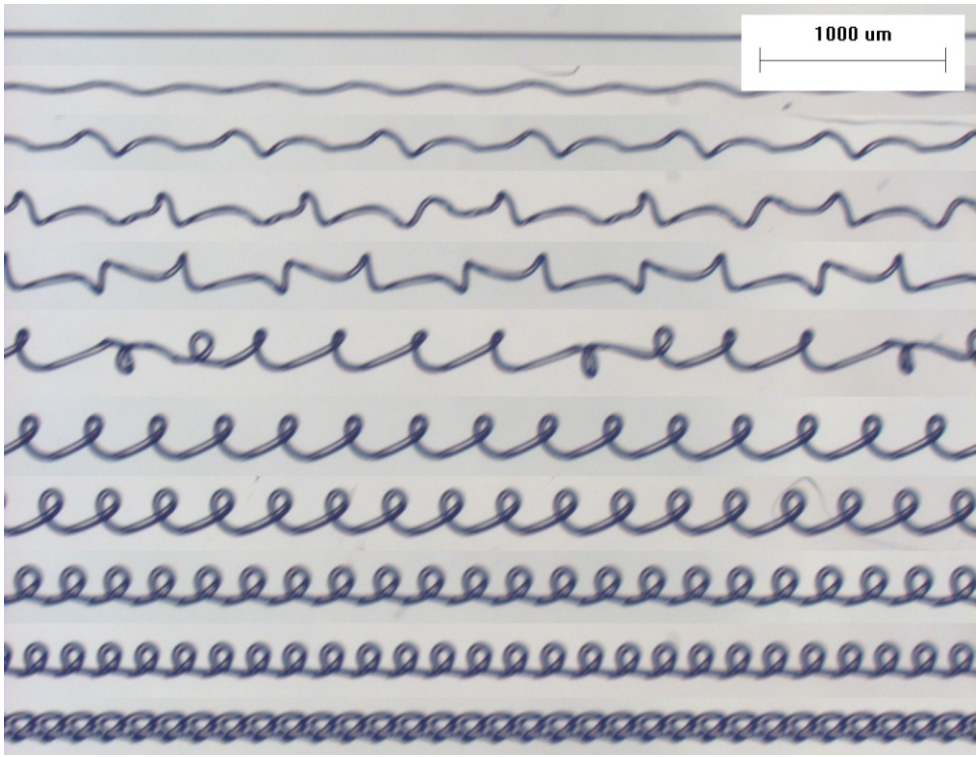

Figure 2-4 Fiber sequence made by Frédérick Gosselin with a $30\mu m$ needle diameter, $300\mu m$ height and substrate speed of 2 mm/s. The jet velocity increases from top to bottom.

Figure 2-5 Example of a thread's diameter measure.

2.3 Uniaxial tension tests

Once the fibers have been produced and their diameters and eventually other useful geometric properties have been determined, the mechanical uniaxial tension test was performed. It was a displacement controlled test without any maximum displacement limit; the goal was to evaluate the material behavior up to its break. The test parameters were: the displacement speed (v) of the machine crossbeam that was 12mm/min and the initial grip separation (l_0), or

theoretical length of thread to be tested, imposed at 20mm. At this position the zeros of the machine ware set, both displacement and force. With these value the initial rate of straining in the test was: $r_{strain} = \frac{v}{l_0} = 0.01\ [mm/mm/s]$. This is the extension velocity $\lambda = \frac{l}{l_0} \rightarrow r = \dot{\lambda}$ which has the same units of measurement as the variation of strain in time $\dot{\varepsilon} = d\varepsilon/dt$. The acquisition frequency was 2.5Hz. The tests were performed on a MTS Insight machine with a 5N MTS load cell and a TestResources grip set with rubber jaws interface specifically bought (Figure 2-6). The thread to be tested was removed from the microscope slide support with a cutter blade paying attention not to break it and trying to prevent any deformation. Using two tweezers it was first clamped into the upper jaw and then into the lower so to avoid any possible pretension.

2.3.1 Data analysis

The untreated results (load-displacement history raw data) are reported in (Figure 2-7). It is possible to remark that all the curves have a very similar shape and the global behavior of the sequence is really repetitive. Out of ten produced threads, with same parameters, seven have acceptable results the other three broke either during removal operation or at the jaws. Of the seven positively tested fibers only a wire produced an earlier break. With a closer look at the first data, a negative displacement is present for all the data (Figure 2-8) due to an internal minimal load threshold of the testing system therefore the threads at the beginning were not really straight. Thus the initial length is the grips separation l_0 and the displacement to reach the minimal threshold load that represents the point where the fiber has started to be tensioned [20].

Since the data were noisy to obtain a better curve a running average on 5 points has been applied. Also the initial and final oscillations were cut considering the first value with positive displacement, which is over the threshold, as starting point and as end the last value before the force became negative, which represents broken thread. The resulting treated force-displacement curves are in Figure 2-9.

Moving forward in the analysis it is possible to appreciate the similarity of different curves shape all characterized by three parts:

- the beginning characterized by a very high slope, representative of the elastic behavior thus Young's modulus,

and by a really reduced displacement, under 1mm, that end with a peak
- the second is a plateau, it arrives to a displacement of approximately 50mm, where the force is almost constant, at a lower value than the previous peak, and is a pure deformation zone. At the beginning of the plateau there is region where the force slowly decreases that probably is when the tension is redistributed on the wire after the first point has yielded
- the third part is the final plasticization with a moderate stiffening modulus, slope, that originate the growth of the load till the break with an appreciable displacement of about 15-20 mm.

The previous analysis highlighted that all threads have a very similar behavior but it can also be inferred a good repeatability because not only the shape but also the values are comparable, in fact this is true for all fibers except the number 4 (Figure 2-9 and Table 2-3). This is the thread that has produced the earlier break; the reason has to be researched in its microscope photos. It was characterized by an important defect: an air bubble, despite the procedure sometime it happens, (Figure 2-10 a). Another irregularity was found in thread number 1: a slight undulation (Figure 2-10 b), due to the variability in the production process as probably the non-perfect level of the substrate or the fact that it was the second thread, the first one broke while detaching from the microscope slide, of the series, sometimes at the beginning the deposition is not yet well stabilized. Nevertheless the presence of undulations, that thread's result is not affected by them. The number 4 will not be considered in next evaluations and analyses so all evaluations will be on six threads and the fact that one out of seven threads has a possible defect which prevent it to work properly will be taken into account in simulations' safety factor.

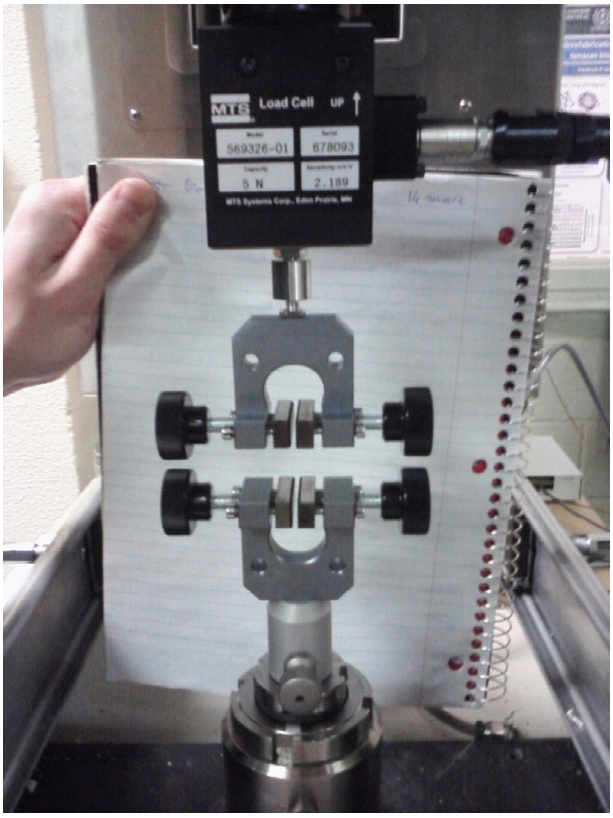

Figure 2-6 Tensile test equipment.

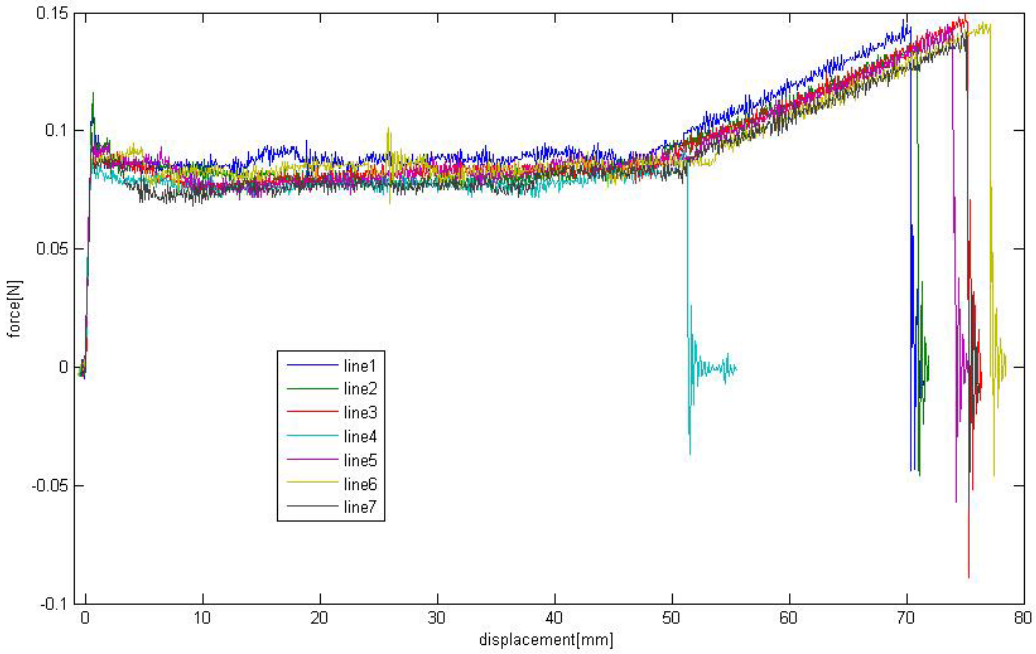

Figure 2-7 Tests raw data: force function of displacement

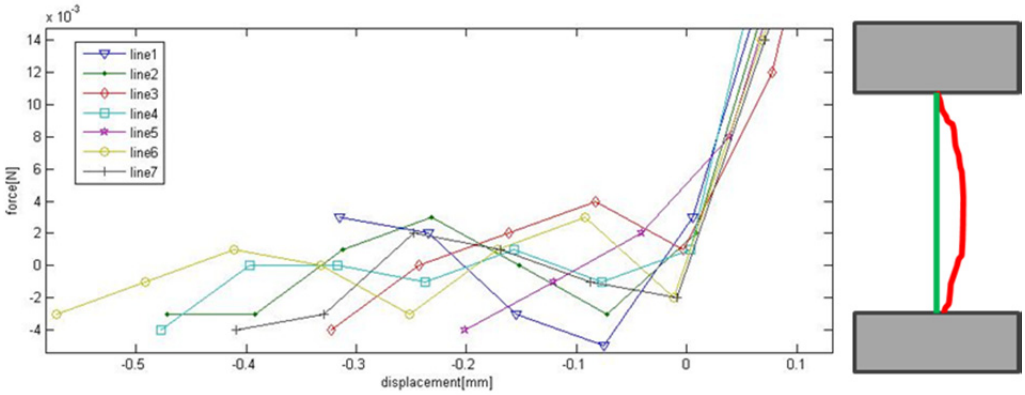

Figure 2-8 Particular of the initial values (right) and drawing of a non-straight clamped simple.

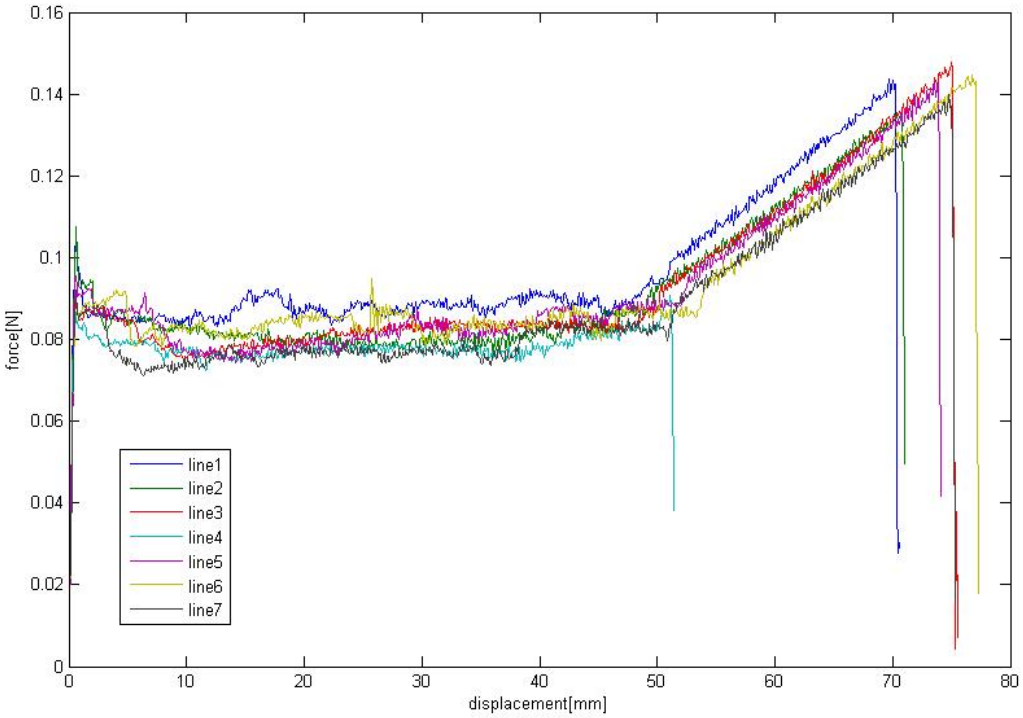

Figure 2-9 Force - displacement curves from smoothed and trimmed data.

Table 2-3 Force and displacement values at break.

threads	Fmax [N]	Displ.max [mm]	Initial length [mm]
line1	0.144	69.685	20.320
line2	0.136	70.808	20.480
line3	0.148	75.037	20.400
line4	0.091	51.123	20.480
line5	0.143	73.879	20.240
line6	0.145	76.788	20.640
line7	0.140	74.792	20.480
Average	**0.135**	**70.302**	**20.434**

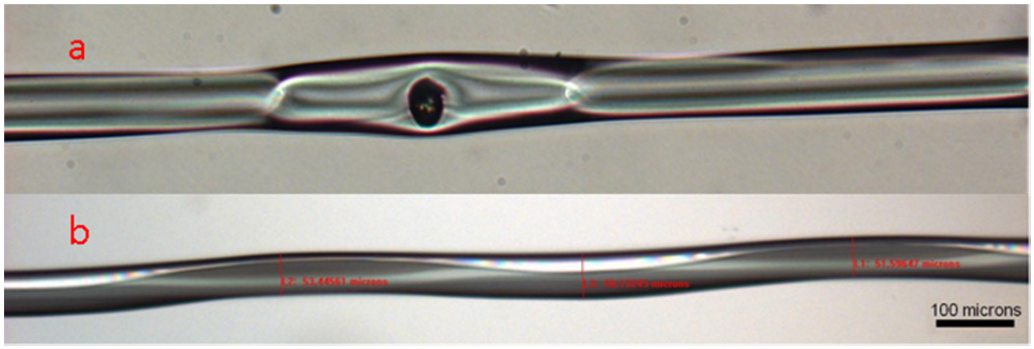

Figure 2-10 a) the air bubble defect in wire 4; b) the undulation defect in wire 1.

2.3.2 Stress - Strain curve

Based on the load history data the stress-strain curve has been evaluated for each thread using its mean diameter, thus under the hypothesis of circular section. As initial lengths it has been used the grips separation, $l_0 = 2\ cm$, plus the clamp error, this is the initial displacement till the load threshold. So the zero load and displacement was established at the linear interpolation between the first positive displacement point and the previous one. Please remember that the fiber number 4 is not taken into account.

With the fibers' geometry the engineering stress $\sigma = F/A_0$ and strain were evaluated as well as the energy to break, i.e. the area under the curve, was integrated and compared with each other.

Working with ANSYS 14.0 as finite element (FE) software and studying the non-linear large deformation of the structure a problem in results compatibility came out. The error between the theoretical values and FE results increased with the global deformation of the structure. This was found to belong to ANSYS' internal material modeling. In fact instead of the classic Cauchy engineering strain model (equation 2-1) the Hencky or true strain is used. Hencky model is based on a logarithmic evaluation of the deformation: it considers the incremental strain and integrates it to obtain the actual strain (equation 2-2). This model gives a better evaluation of the deformation when it takes place in a series of increments as it appends in the iterative algorithms of a non-linear solution but also in reality. The conversion between the Cauchy and Hencky strains is given by (equation 2-3).

$$\varepsilon = \frac{\Delta l}{L_0} = \frac{l - L_0}{L_0} \qquad 2\text{-}1$$

$$\varepsilon_H = \int_{L_0}^{l} \frac{\delta l}{l} = \ln\left(\frac{l}{L_0}\right) \qquad 2\text{-}2$$

$$\varepsilon_H = \ln(1 + \varepsilon) \qquad \varepsilon = e^{\varepsilon_H} - 1 \qquad 2\text{-}3$$

Thus in all evaluation procedures, the Hencky's strain definition was applied and the material's curves for tests results were obtained (Figure 2-11).

To implement the material properties into a FE model a non-linear model was necessary and a multilinear was the more correct representation. The definition of this material representative curve was not evident at first but resulted the easier and more effective way to use directly the test data in FE simulations. Thus it has been obtained by linear regression. Indeed the multilinear model was inferred with the average of the transition points between each curve's zones. An absolute definition of these points was not possible so the better way to obtain them was with a linear regression for each part of every curve. This way, for each tension curve three different lines were representative of the global behavior. Transition points were defined at the interception of the two adjacent regression lines; to obtain the final multilinear material model the average of all curves at each transition point was evaluated, both stress and strain values.

Breaking energy of the multilinear model has been compared to the tests average value with a reasonable result since the difference between tested threads' average energy and multilinear model is less than 2% (Table 2-4 and Figure 2-12). The fact that the multilinear model has a lower breaking energy than the average could be seen positively as a safety factor indeed a greater value should be considered risky. Thus it is possible to assert that the obtained curve is representative for the study purpose: to employ the threads in order to absorb the kinetic energy of an object, this is using the breaking energy of the fibers in a structure. To make the most out of the material behavior, it should be taken advantage of its large deformation capability so the resulting web structure will absorb energy allowing a large perpendicular displacement, not ideal for a bullet-resistant vest but still good for other applications. Another method to evaluate the web performance with breaking energy is the quantized fracture mechanics that works for failure in discrete structures [12].

The multilinear model has been further simplified to a linear elastic material with equal breaking point (Figure 3-1). Thus it is possible to compare the influence of the material behavior on the web resistance.

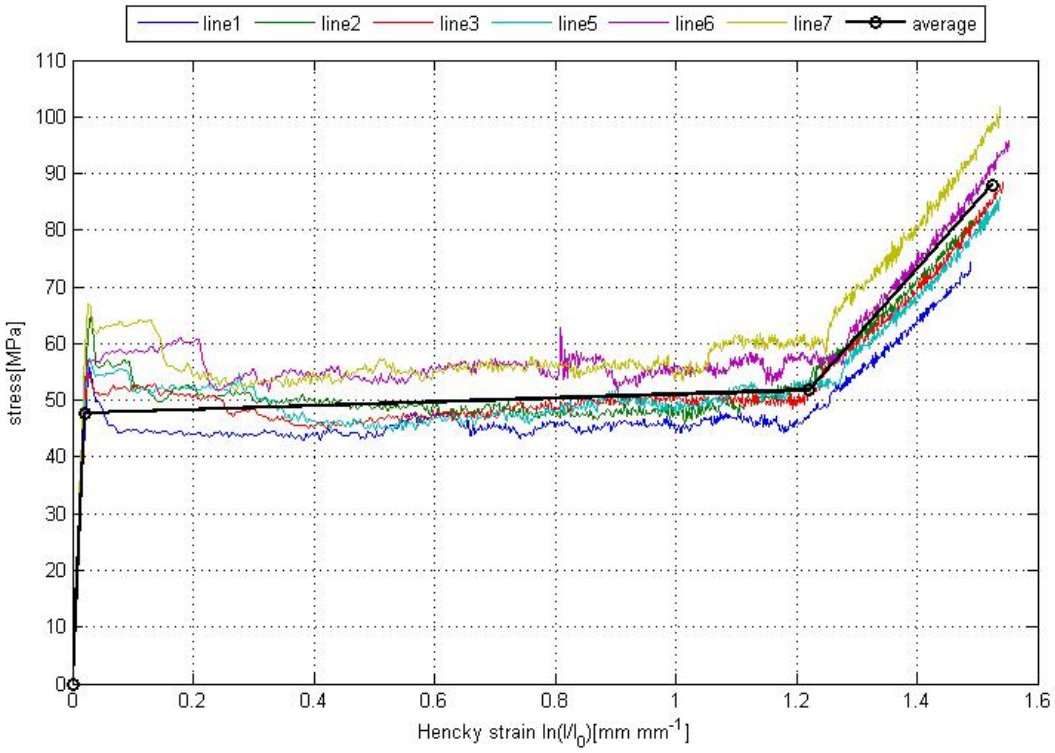

Figure 2-11 Stress –Hencky strain curves with the multilinear model (average).

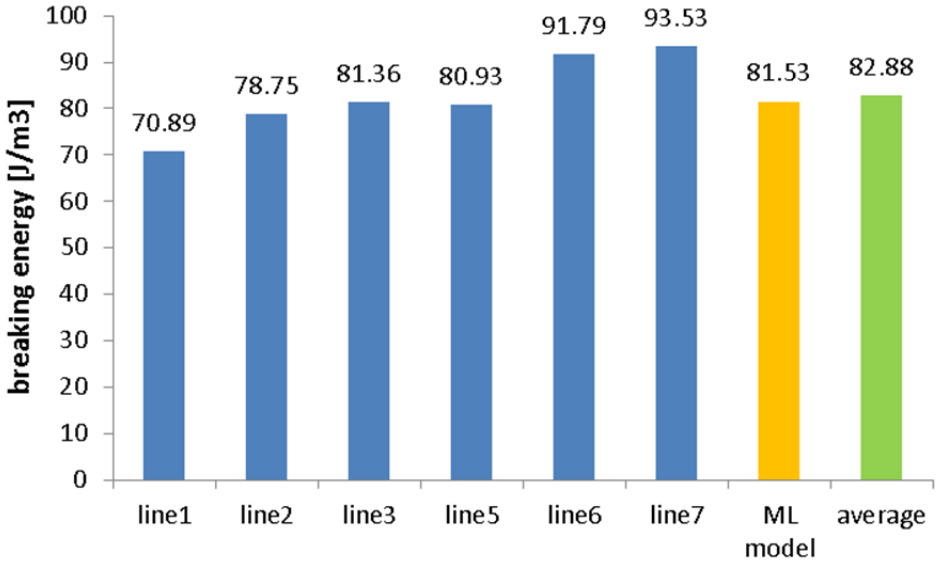

Figure 2-12 Breaking energy of the different fibers and of the multilinear model (ML) compared to the average of simple's values.

Table 2-4 Breaking values of the tested fibers with the multilinear (ML) representation model and the fibers' average and standard deviation.

Threads	Breaking			
	Energy [J/m^3]	Stress [MPa]	Hencky Strain ε_H [%]	Cauchy Strain [%]
line1	70.89	74.35	1.49	3.43
line2	78.75	81.80	1.49	3.46
line3	81.36	88.55	1.54	3.68
line5	80.93	85.73	1.54	3.65
line6	91.79	95.72	1.55	3.72
line7	93.53	101.79	1.54	3.65
ML model	**81.53**	**87.99**	**1.53**	**3.60**
average	82.88	87.99	1.53	3.60
std	8.48	9.80	0.03	0.12

Chapter 3. FEM modeling and results

The goal of finite elements study was to develop a tool for structural testing on a geometry inspired by spiders' orb-webs. The study is characterized by the presence of two non-linear aspects: the very large deformation of the structure that implies a geometric nonlinearity, and the material which, as already shown in Chapter 2, has a non-linear behavior. The combination of material production, mechanical testing, data analysis and finite element models provides a complete methodology of study that can be reapplied on different fibers, using almost the same procedures and algorithms, to compare the results, create new geometries or load situations.

In this chapter the structural verification under a static load is described. Previously two material models have been deduced (Figure 3-1): the multilinear non-linear model that represents the real material behavior whereas the linear is a simplification to study the material influence (as in [12]). Here two analytical models of a single wire structure will be developed for both situations of a center and an off center load; they will be used to understand and compare the FE results before the analysis of more complex geometries.

3.1 Analytical models

In order to have a better understanding and a critical view on the Finite Elements (FE) simulations the following simplified models with two different load situations have been considered. They study the static equilibrium of a single fiber under the effect of a perpendicular action, force or displacement, which simulates a mass attached on a double hanged wire. This external load could represent an insect on a spider web. The two cases that have been studied are when the action is in the middle point of the fiber's length and when it is off center.

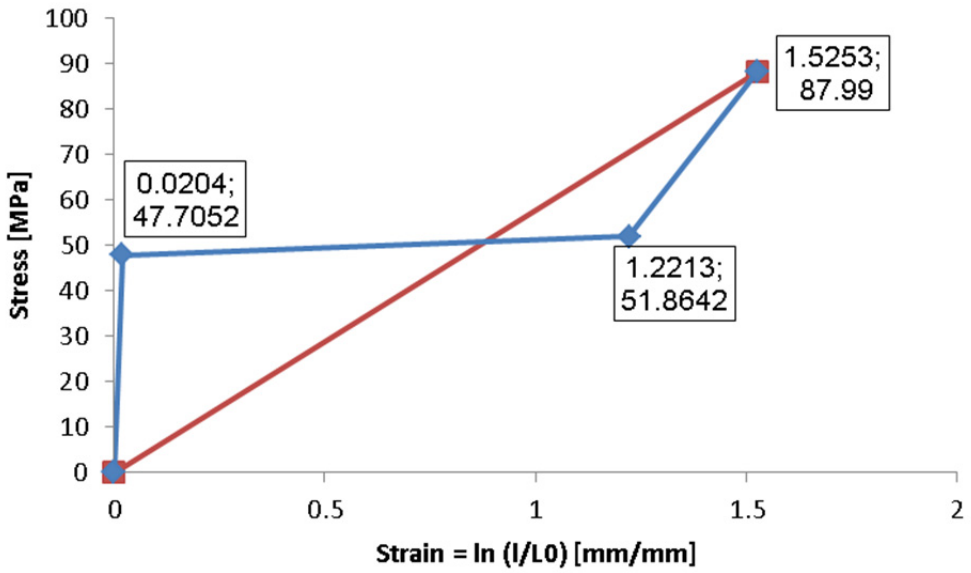

Figure 3-1 Material models: multilinear (bleu) with the points' coordinates and linear (red).

3.1.1 Load at the center

The first case is the simplest and can be solved using only the vertical static force equilibrium equation that for a centered load on a thread is:

$$F = 2\,T\sin(\theta) \;\; ; \;\; 0 \leq \theta \leq \pi/2 \qquad 3\text{-}1$$

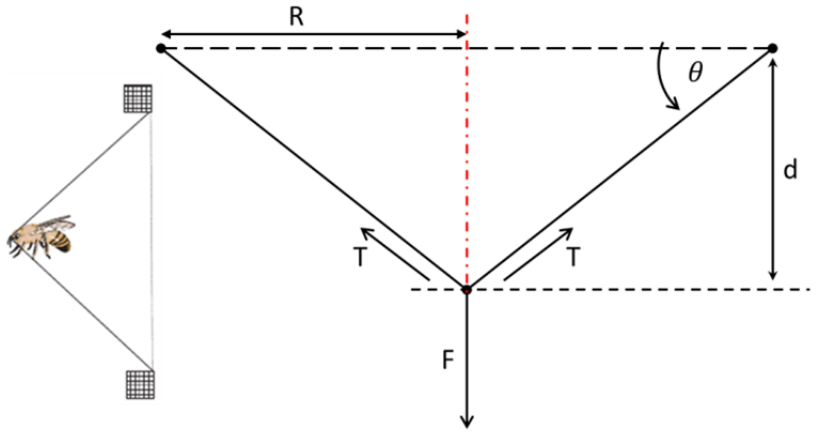

Figure 3-2 The central load structure with the external force (F) and the displacement (d), on the left a drawing of an insect collision.

Where F is the external action like a weight, T is the tension in the threads and θ is the angle between deformed and undeformed configurations (Figure 3-2). Considering the material and geometric properties it is possible to write also:

$$T = A\,\sigma = AE\varepsilon_H = AEln\left(\frac{l}{L_0}\right)\ ;\ L_0 = R \qquad 3\text{-}2$$

$$l = \frac{R}{\cos(\theta)} = \frac{d}{\sin(\theta)} = \sqrt{d^2 + R^2} \qquad 3\text{-}3$$

$$\tan(\theta) = \frac{d}{R} \rightarrow \theta = \tan^{-1}\left(\frac{d}{R}\right) \qquad 3\text{-}4$$

These equations can be used to evaluate directly the force that would cause an imposed displacement d, knowing the thread's cross-section A, its initial length $2L_0$ that is the same as the double of the radius R and the material Young's modulus E, if the linear model is considered otherwise with the multilinear it has to be applied the modulus of each different model's zone. Because of the different definition of the strain the classic equivalence between an elastic fiber and the tension in a spring is no more possible, indeed if a characteristic constant $k = \frac{EA}{L_0}$ is possible with Cauchy when Hencky is used the tension could not be reduced under the form $T = k\Delta l$.

With the perpendicular action applied in the middle the work required to deform the fiber reflects the behavior of the material obtained under a simple uniaxial tension. Indeed when the force, as function of the perpendicular displacement, is considered the resulting graph is very similar to the material's one. Moreover, the strain where the areas under two different material's tension curves, as linear and multilinear, is equal, i.e. the deformation energy is the same, remains the same also in the transversal situation.

Both deduced material models were used to obtain the analytical solution imposing a range of perpendicular displacements and evaluating the related force to produce such movement. The horizontal equilibrium of the structure is innate because the two angles at the base of the triangle, resulting from the deformed configuration, are equal, it is an isosceles triangle, as are also the fibers' tensions.

This configuration was already analyzed for spider's silk in [1] demonstrating how the mechanical properties of silk locate it in almost optimum conditions for maximum sustainable force (Figure 3-3). Indeed even though in transversal configuration the tension in the fiber is higher than in a simple uniaxial tension due to the angle, when the maximum sustainable load is evaluated the MA silk is close to the optimum while the viscid silk is well beyond because it has to absorb the prey's kinetic energy reducing de deceleration by greater extensibility.

The same curve has been obtained for this study tested material with the evaluation of the final stress (σ_f) on section area (A_f) function of the extension (l_f/R) instead of the engineering stress used before here called (σ_{ML}).

$$F_{max} = 2T\ sin\theta = 2\,\sigma_f A_f\, sin\theta$$

With l_f the final length of the fiber and the equations:

$$sin\theta = \frac{\sqrt{\left(\frac{l_f}{R}\right)^2 - 1}}{l_f/R}\ ;\ l_f = e^{\varepsilon_f} \cdot R$$

$$A_f = \frac{A_0 R}{l_f} \rightarrow\ \sigma_f = \frac{T_{ML}}{A_f} = \sigma_{ML}\frac{l_f}{R}$$

The sustainable force can be written as function of l_f/R:

$$F_{max} = 2\sigma_f A_0 \frac{\sqrt{\left(\frac{l_f}{R}\right)^2 - 1}}{\left(\frac{l_f}{R}\right)^2}$$

Resulting in (Figure 3-4) with a similar position as spider's viscid silk. The optimum Hencky strain to resist static loads is between 0.2 and 0.6.

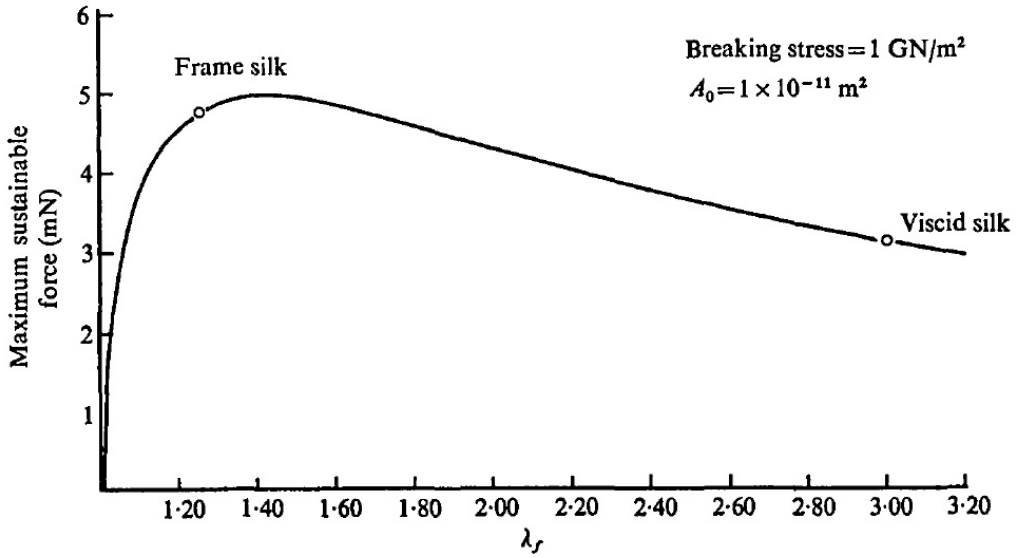

Figure 3-3 Theoretical maximum sustainable force for a transversal load on a fiber for given σ_f. The λ_f is the extension ratiol_f/l_0. Taken from [1]

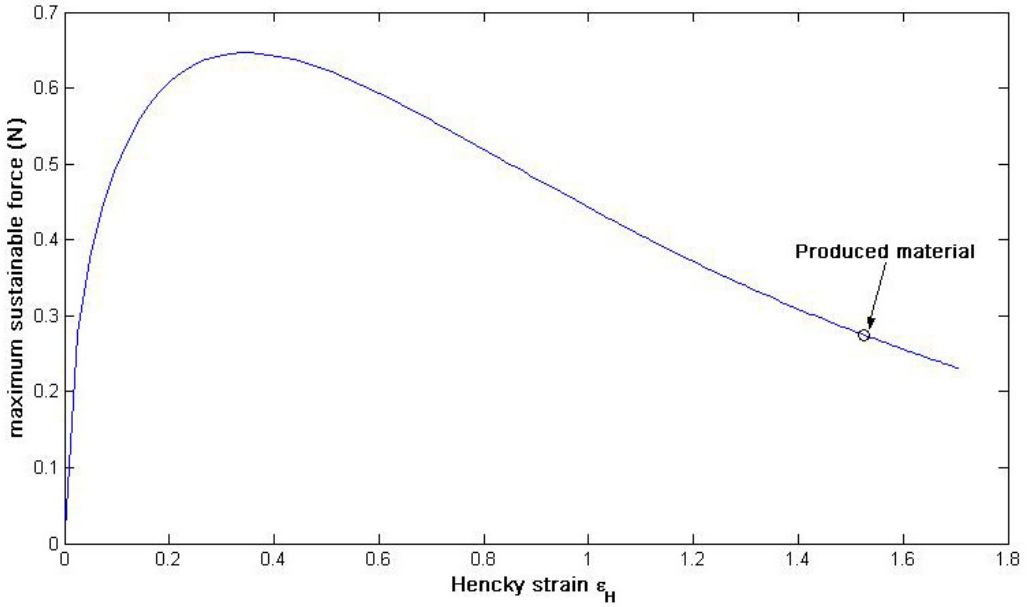

Figure 3-4 Maximum theoretical sustainable force for produced material properties and its location.

3.1.2 Off center load

To evaluate the effect of a force that is not perfectly in the center of the structure a different model is developed considering the hypothesis that the load action is on a fixed point, which does not change like a mass strictly attached to the fiber, and the direction is always vertical as the gravity.

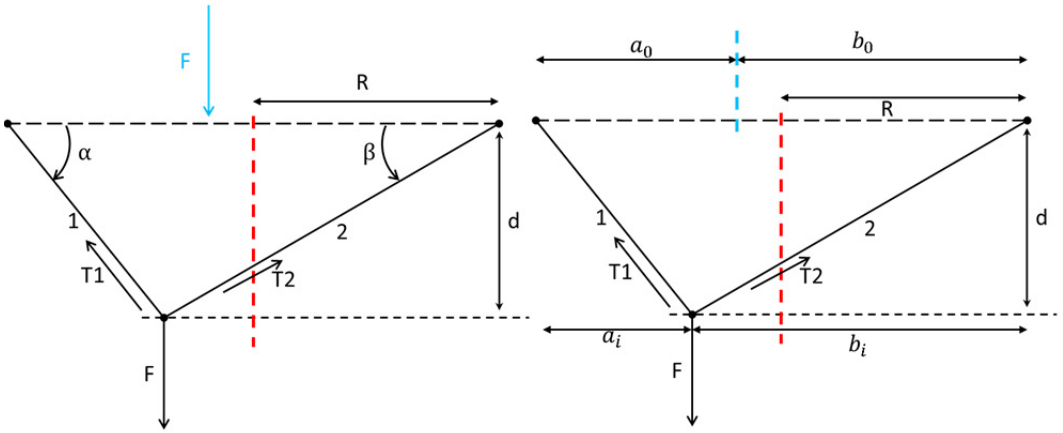

Figure 3-5 Off center load diagrams: the red line is the center while the blue line is the initial load application line.

The diagram of this situation is represented in (Figure 3-5) and, as before, a static study is developed with equilibrium equations in vertical and horizontal directions. It is important to remark that in this model the angles made by the deformed structure at the joints are not equal, this is due to the off center position of the load that creates an unbalanced horizontal situation. The system of equations has linked variables and its solution was made with an iteration procedure.

There are two components to satisfy in the system: the geometrical congruence and the force equilibrium.

First the geometric problem:

$$a_0 + b_0 = 2R = a_i + b_i \qquad 3\text{-}5$$

$$l_{1i} = \frac{a_i}{\cos\alpha} \; ; \; l_{2i} = \frac{b_i}{\cos\beta}$$

$$l_{1i}\sin\alpha = l_{2i}\sin\beta = d \qquad 3\text{-}6$$

Where $a_0, b_0, 2R$ are respectively the initial lengths of the left side, right side and the total length between joints; l_{1i}, l_{2i} are the length of the two deformed elements; $\alpha; \beta$ are the angles of the deformed configuration and d is the perpendicular displacement. The eq.3-5 is the horizontal congruence and the relation for the vertical congruence is set in eq.3-6.

The force equilibrium is given by:

$$T_1 \cos\alpha = T_2 \cos\beta \quad 3\text{-}7$$

$$F = T_1 \sin\alpha + T_2 \sin\beta \quad 3\text{-}8$$

Where T_1, T_2, F are the tensions in the two thread's elements and the applied force. The eq.3-7 represents the horizontal equilibrium and the eq.3-8 the vertical. As for the centered load the tensions can be written as function of the stress and strain (eq.3-2) this time with different L_0, for the two sides respectively a_0 and b_0 .

Another formulation of the equation system for this problem can be obtained based only on lengths instead of angles thus it is more accurate under the numerical point of view and also faster to solve.

From the geometry we have:

$$a_0 + b_0 = a_i + b_i \quad 3\text{-}9$$

$$d^2 + a_i^2 = l_1^2 \quad 3\text{-}10$$

$$d^2 + b_i^2 = l_2^2 \quad 3\text{-}11$$

And transforming the cosines and sines of angles in the ratios of the sides the force equilibrium becomes:

$$T_1 \frac{a_i}{l_1} = T_2 \frac{b_i}{l_2} \quad 3\text{-}12$$

$$F = T_1 \frac{d}{l_1} + T_2 \frac{d}{l_2} \quad 3\text{-}13$$

The iterative algorithm is based on the knowledge of the final desired displacement D and in addition to start the solution an arbitrary small difference from a_0 is imposed for the value of a_i, it is the first

iteration point in which geometry is known and only the force equilibrium has to be solved. Then based on the result of the first two iterations the real solution is researched. First the geometry is solved and lengths b_i, l_1, l_2 (from Eq.3-9,3-10 and 3-11) are calculated so the strain of each segment can be evaluated and, with the material law, also the tensions become known (Eq.3-2). To verify if the geometry satisfy also the force equilibrium the horizontal equation is considered (Eq.3-12). Until it results under the desired tolerance, the value of a_i is changed according to a linear interpolation of previous results to reach the zero of the error between the two horizontal components of the tensions. The force that produces the displacement D is then calculated with the vertical equilibrium (Eq.3-13). Of course this procedure can be done in a loop thus to find the equilibrium points from an initial value for D_{strat} to D.

3.1 Structural design

The goal here is to find the breaking value for the material under a perpendicular load. The design parameter is the maximum strain of the fiber, as the material properties suggest, and it is enough to calculate the geometry at break. The design was made on the centered load model to define the maximal displacement and in the case of a radial structure the number of radii (Figure 3-12). The obtained results were applied also in the off center case.

For a load at the center and a given breaking strain the maximum perpendicular displacement can be calculated based only on the geometry with the definition of the strain (eq.2-2 and 3-3). To take advantage of the material the best thing is to have a large deformation for this reason the design is made near the break.

$$l_{Max} = e^{\varepsilon_{HMAX}} \cdot R \rightarrow \ d_{Max} = \sqrt{l_{Max}^2 - R^2}$$

With the tests' values $\varepsilon_{HMAX} = 1.525$, $R = 40mm$ the breaking displacement is $d_{max} = 179.40\,mm$ that means a force of $0.276N$ for a single fiber. This is the same as in (Figure 3-4). Considering a safer strain as the 90% of the final strain it becomes: $\varepsilon_{H_{0.9}} = 1.373$ and $d_{max} = 152.74\,mm$. The load value at this new limit for the multilinear model, which is the only reasonable in this case, is $0.215N$.

Based on the previous results it is possible to evaluate the number of radii required in a pure radial system to support a determined weight without exceeding a prefixed maximal deflection. The radial structure is symmetric so it can be analyzed with the simple model already developed considering the fact that the force in the simple model now becomes equal to the total load divided by the number of diameters, half the number of radii, present in the structure. Thus it is possible to design the number of radii:

$$N_d = \frac{N_r}{2} = \frac{F_{tot}}{2Tsin(\theta)} = \frac{F_{tot}}{2AE\ \varepsilon_H \sin(\theta)}$$

Using the $\varepsilon_{H0.9}$ and the linear material model the following results were obtained:

Table 3-1 Number of radii needed to support different forces.

total Force [N]	Ndiameter	Nradii
2	8.4	16.8
2.5	10.5	21.0
3	12.6	25.2
3.5	14.7	29.4
4	16.8	33.6
4.5	18.9	37.7
5	21.0	41.9

The number of radii was so chosen to be 40 because it is even, thus the structure remains symmetric, and the angle between the radii is integer ($\gamma = 9°$). Since the linear model of the material has higher stress values at the end, the force value is not exact but still gives an idea: with 40 radii and the multilinear model the load results $F_{sym} \cdot N_d = 0.215 \cdot 20 = 4.3\ N$.

An additional safety factor could be considered to cover the presence of defects in the fibers: based on the tests' results one fiber out of seven had a defect that caused an earlier break.

For the off center situation the same number of radii is used because it is not possible to make an evaluation since there is no more structure symmetry.

In all cases the structures are tested till the first fiber breaks.

3.2 FEM approach

Before models description, some considerations of general validity to the study are presented. They concern the nature of the problem and how it can be simulated with the FE method.

Being the web made by fibers and considering that a wire has only the axial component of the stress tensor the FE model was realized with truss elements, LINK180 in ANSYS. Truss elements have two nodes with three translations as DOF, inside the element there is no variation of the axial stress and axial strain thus a finer mesh does not produce more accurate results. The simulation of an external perpendicular action on the structures could be done following two different approaches: imposing a known force or an off plane final displacement to the structure. A simulation based on force as input requires an additional element to create the initial resistance otherwise the load has no effect on the DOF of truss elements. The explanation is that although the element's nodes have three DOF, one in the same direction of the load, for the initial deformation the force is applied but in a perpendicular direction to the element axis and on that direction the element stiffness is nothing. The solving equation in that direction has no DOF, because it is multiply by the stiffness (eq.3-14), so there is no movement in the space which would cause an element deformation. Instead with a final displacement approach no extra element is needed because the displacement is directly associated with the DOF so it generates a movement. With this approach the solution is faster being direct: the DOF is set and the resulting force is evaluated. The displacement method has a large advantage so this is the method used.

$$[K]\,\boldsymbol{u} = \boldsymbol{F} \qquad 3\text{-}14$$

Element properties were fixed for all the cases in the study. Directly related with the element used is the Poisson's ratio set to zero because the LINK180 element does not consider it in the

computation, this reduced the amount of information required, otherwise an evaluation should have been done. No mass per length unit was considered because it has only influence in the dynamics. In reality if a fiber is hanged at its ends it does not remain straight but it bends under the effect of its own weight. Since a wire has no bending moment, to keep it straight a tension should be applied like in guitar's strings generating so a bending resistance. The elements' cross-section is the same for all elements and it is calculated from the average diameter of fibers thus it has the value of $0.0016\,mm^2$. Moreover, the cross-section of the element is assumed to be rigid so there is no scaling related to the axial stretch in order to maintain the total element volume constant, i.e. the material volume. For a looped fiber this assumption can be done because the hidden length of the loop changes the total volume under stress when the bond is broken; but for a straight fiber it is not the case. The material behavior is based on the engineering stress, thus the initial section is considered when the stress is calculated; the evaluation of the necking phenomenon on the fibers was not considered at this point so a rigid section is assumed also in the test data analysis and it results in the stress/strain curve used for the FEM model.

The material was represented at first as linear by the Young's modulus of the breaking point (Figure 3-1). Then a multi linear representation was realized with the MISO (Multilinear Isotropic Hardening) material model in ANSYS. The advantage of MISO is that it is possible to directly use the coordinates of the characteristics points of the non-linear curve obtained before. The MELA (Multilinear Elastic) material model present in the user interface is not recognized by the LINK180 element.

Same constraints were applied for the different models: like in a circular support only the external circumference of the web model was fixed. It is a radii extension beyond the spiral last turn, like in real spider webs, to attach the web to an external rigid frame. In simulations this frame is constituted by a circle with diameter of 8 cm thought to be used in experimental tests. This means that all external circumference nodes had each DOF constrained; in case a force was imposed also the additional element had the other end fixed.

3.3 FEM simple models

First the cases of a single fiber were simulated and compared with the analytical solutions.

3.1.3 Load at the center

This model is constituted of two identical aligned elements of length $R = 40\ mm$, the imposed displacement on the middle node changed in a range under the limit of $150\ mm$ as designed to prevent the material break going beyond the limit of $\varepsilon_{H0.9}$. The results of the force required to obtain a specific displacement are illustrated in (Figure 3-6) and show a perfect coherence with the analytical results for both the linear and multilinear material models. The analytical curves arrive to the material breaking point associated to ε_{HMAX}. The graphic point out also how the different material behavior is reflected by the force: the multilinear has higher stress values for small displacement than the linear model exactly like the obtained force trend.

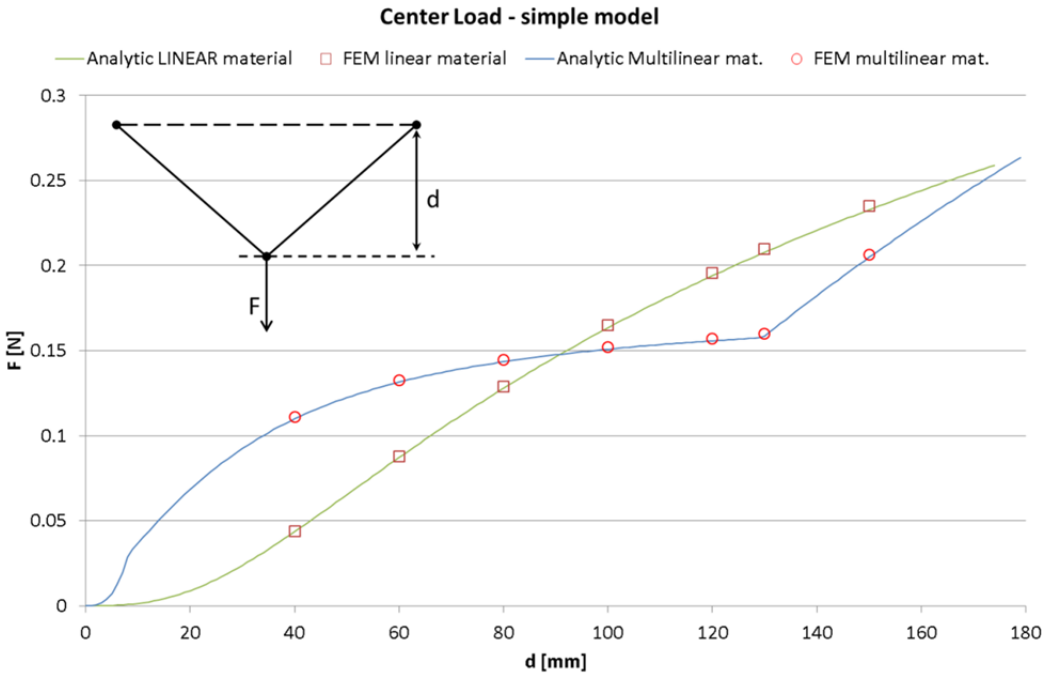

Figure 3-6 Analitycal solutions and FEM results in the case of load applied at the center for a single fiber structure.

Table 3-2 Analitycal and FEM resulting values in the case of load applied at the center for a single fiber structure.

Displacement [mm]	Hencky strain	Force[N]			
		linear material		multilinear material	
		analytical	FEM	analytical	FEM
150	1.356	0.233	0.235	0.205	0.206
130	1.224	0.208	0.210	0.159	0.160
120	1.151	0.194	0.196	0.156	0.157
100	0.991	0.163	0.165	0.151	0.152
80	0.805	0.128	0.129	0.143	0.145
60	0.589	0.087	0.088	0.131	0.133
40	0.347	0.044	0.044	0.110	0.111

3.1.4 Off center load

Like the previous model this one has two elements but this time their lengths are different: the application point of the displacement is at 25% of the total length, i.e. it is at 20 mm from the left that is at the half of the previous radius R. The shorter element, the one on the left, will be called the element 1 (el.1) while the other is the element 2 (el.2), (Figure 3-5), this to explain the behavior in the results. The first aspect to consider is the path made during the movement by the point where the displacement, or the force, is applied. In (Figure 3-7) are shown the two different trajectories in the case of linear material, on the left, and multilinear material; on the right. Note that the coordinate x is the horizontal movement equivalent to the variation of the dimension a_i while the y is the perpendicular displacement d. In (Figure 3-8) the FE iteration points area shown and the analytical solution for the linear material is compared. With the linear material model the FE solution is coherent with the analytical: the application point at the beginning move to the left because the el.1 has an higher

initial rigidity so a greater tension, then it returns on the vertical line of the initial displacement application due to the angles (α, β) and, even if the material breaks before (see Figure 3-7), the point goes farther on the right. Thus with a perfectly vertical off center load applied on a point the solution shows the presence of a horizontal action that modifies the final position so it is no more in line with the initial point of load.

For the non-linear material there are two series of points describing similar trajectories: they are two different solutions of the same case but with different iterations number imposed to the solver. The faster solution has a less accurate result with an oscillation and a final equilibrium point that is a little bit over the material break condition. The path obtained with the non-linear material is completely different from that of the linear material. This is due to the stress in the two elements (Figure 3-9). Analyzing the path and the related stresses in the elements it is possible to understand why it happens. At the beginning, for y less than 10 mm, the point moves to the left, like in the linear material, and it is when both elements are in the first elastic part of the material curve. After in the trajectory there is a knee and the point moves to the right because the el.1 has entered the material plateau so its stress does not change with the increasing of strain. Meanwhile the el.2 still has an elastic behavior, and it will never enter the plateau. When the stress in the el.1 reaches the final and stiffening part of the material's curve, at around 60 mm of perpendicular displacement, the point, where the external action is applied, returns to the left because of the higher tension in the el.1. The stress concentration in el.1 and the fact that el.2 never exceeds the yield reproduces exactly the behavior pointed out in the introduction by [12]: only the sector of the orb web where the load is applied reaches the final stiffer trait of the stress-strain curve.

In (Figure 3-10) force on the displacement curve shows a new behavior with the multilinear material always requiring a greater force than the linear. Comparing the off center case with the centered one we note that the perpendicular displacement at break is lower, under two-thirds of the central one. This is due to the intensification of the stress in the shorter element. The off center case requires a greater force to deform it at an equal perpendicular depth. The general trend of each material model is somehow respected but, this time, their relative behavior is not: they don't cross each other.

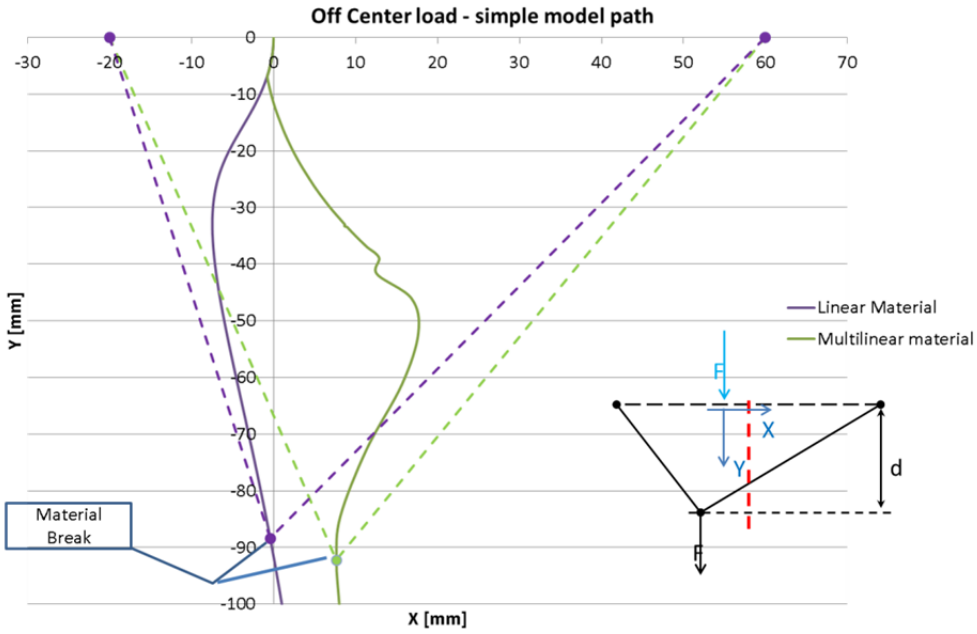

Figure 3-7 Off center load: the trajectory made by the external action application point (continuous line) for the linear and multilinear material models. The dashed lines represent the deformed structures at break.

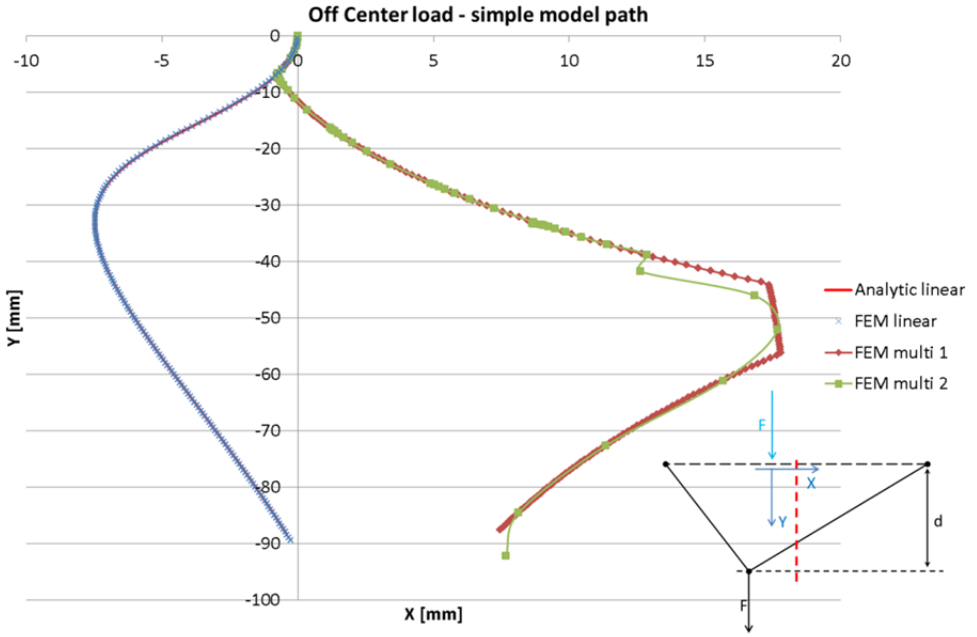

Figure 3-8 Off center load, external action simulated path: The linear material correspond exactly to the analytical solution. Two simulations for the multilinear material are presented the green was obtained with less iteration and has a final displacement value greater than the material break.

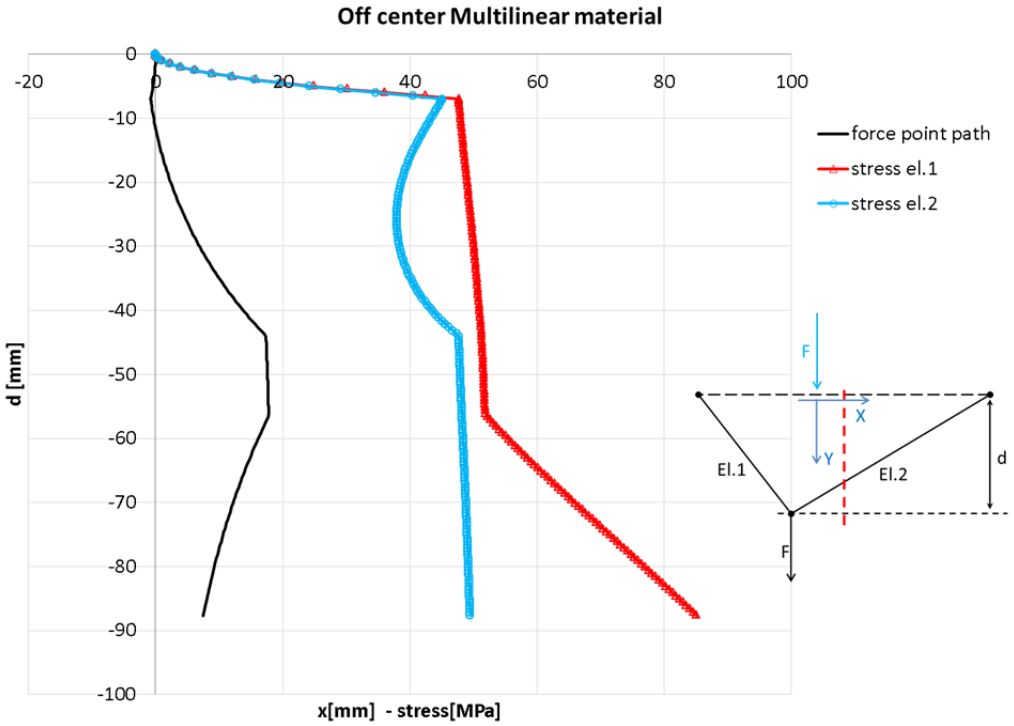

Figure 3-9 Elements' stress analysis during the deformation under an off center load.

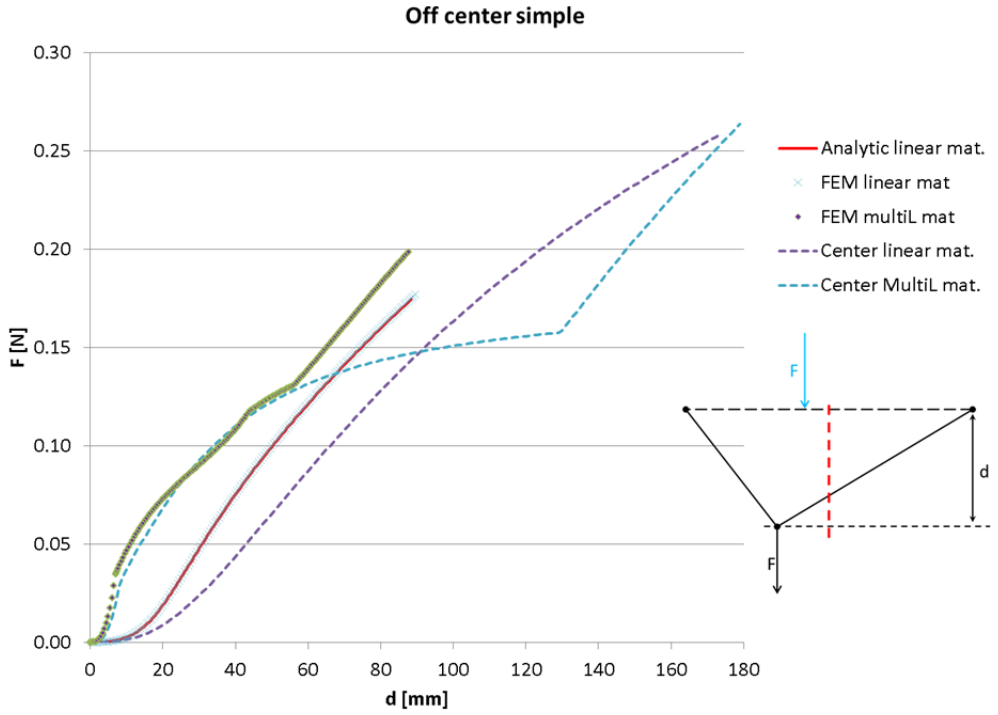

Figure 3-10 Off center simple model: force vs. displacement until material break.

3.4 FEM web models

Now after that the simple models were verified and understood, the simulation moves forward increasing the complexity from an only radial model to the complete geometry reproducing the spider's web with radii and spiral (Figure 3-12). Once again the study was conducted for the two material models and load situations. The spiral used in this study is characterized by balanced distance between two consecutive turns and the length of the arch between two radii of the web (eq.3-15). This was thought to reduce eventual problems of high element size differences. The modulus of the radial distance $\rho(x)$ is function of the angle x in the turn and of γ that is the spacing of structural radii, i.e. the angle between the radii of the web. Changing the number of radii the spiral will be modified: a reduced radii number results in less spiral turns with larger space between each turn. The spiral equation becomes therefore (eq.3-16). The spiral is then adjusted to obtain the desired dimensions as initial and final radial distance, in the simulations the maximum diameter of the spiral was 70 mm and the starting diameter was 10 mm; the radii are always 40, as previously calculated, if not it will be remarked.

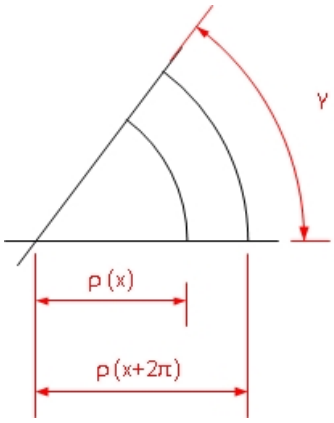

$$\rho(x + 2\pi) - \rho(x) = \rho(x) * \gamma \qquad 3\text{-}15$$

$$\rho(x) = e^{\eta x} \text{ with } \eta = \frac{\ln(\gamma+1)}{2\pi} \qquad 3\text{-}16$$

Figure 3-11 Equilibrated spiral caracteristics

The models made only by radii, called radial models, have one element for each of the structure radii, thus with dimension R, for all but the radius on which there is the point of application of the displacement. This radius is divided in two elements: from the center to the action point and then to the external circumference. When the spiral is added the elements become one each line segment of radii or

spiral between any intersections. The number of elements increases significantly for small γ leading to difficult solutions.

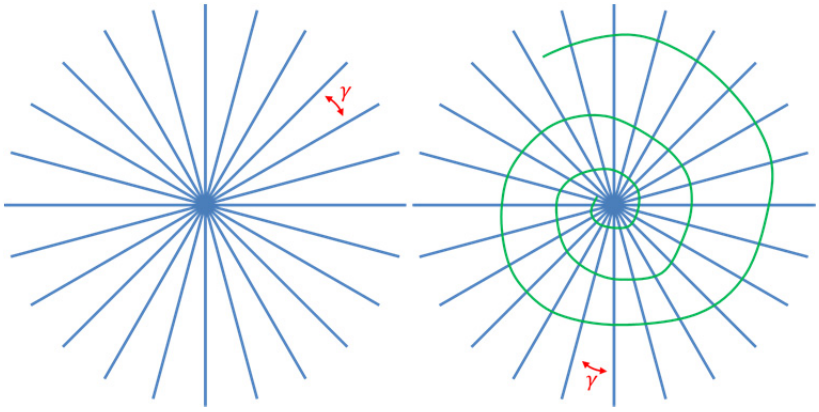

Figure 3-12 Web schematic models: only radii spaced by γ on the left and with spiral on the right

3.1.5 Load at the center

The simulations of the radial model can be directly compared with the simple model with the load at the center thank to the symmetry of the structure. Thus multiplying the results of the single wire by the half of the number of radii the evaluation can be done. The comparison between the case only with radii, the analytic solution and the case with the added spiral is shown in (Figure 3-13). It is evident that when the load is applied at the center the spiral has no function indeed the stress is equally distributed only on the radii (figure). The different material models have the exactly same behavior as in the simple center case. Thus it is possible to affirm that the spiral has no role in supporting the load when this one is in the middle of the radial structure.

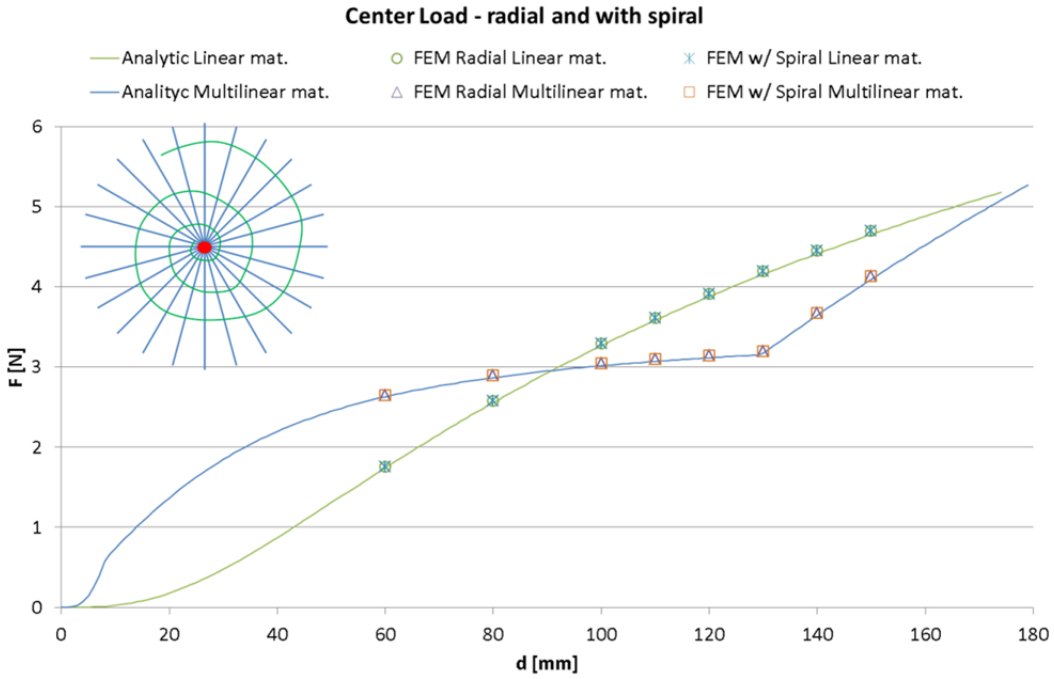

Figure 3-13 Load at the center on the web structure: the spiral has no influence.

3.1.6 Off center load

When the load is placed at a distance of half the structure's radius the importance of the spiral appears. In the generation code the action point was chosen between the existing points: the load was applied on the closest existing node. In this case the presence of the spiral increases significantly the force needed for an equal transversal displacement. Before the pure radial structure under the off center load was simulated and gave results similar to the simple fiber situation; there is no increasing of the force value because the structure has no symmetry in this configuration. The difference with the single fiber is that half radius works alone while the other part is supported by all the radii (figure). To remark is the fact that the linear and the multilinear material cross themselves, in contrast with the single fiber, and that the multilinear seems to break down first, the point at 90mm could be just a numeric effect.

The simulations of the complete structure, with the spiral, have been done for different numbers of radii because the solution of the 40 radii structure was difficult to find due to the elevate number of elements. Thus first an easier solution was researched for a reduced number of elements, this is increasing the angle γ to reduce the radii

and the spiral length. Even though the webs had fewer radii than the pure radial structure the force increases and reaches more than its double with half radii at equal displacement.

As the number of radii grows also the force grows but the structure breaks earlier: it arrives to break at a displacement of 60 mm instead of the 90 mm of the radial structure with same linear material but the load has more than doubled.

When adding the spiral the result is a structure able to support a higher force at equal displacement, thus more work done that is higher energy absorption, or higher force with lower perpendicular deformation at break, reducing the penetration (Figure 3-14). Comparing the results with the centered load two main differences have to be noticed: the force is several times lower and the perpendicular deformation is just a bit over the half (Table 3-3). This means that the structure is optimized for a load at the center, indeed is a radial geometry so at the center all radii work in parallel. But it can support also lower off center charges thanks to the spiral.

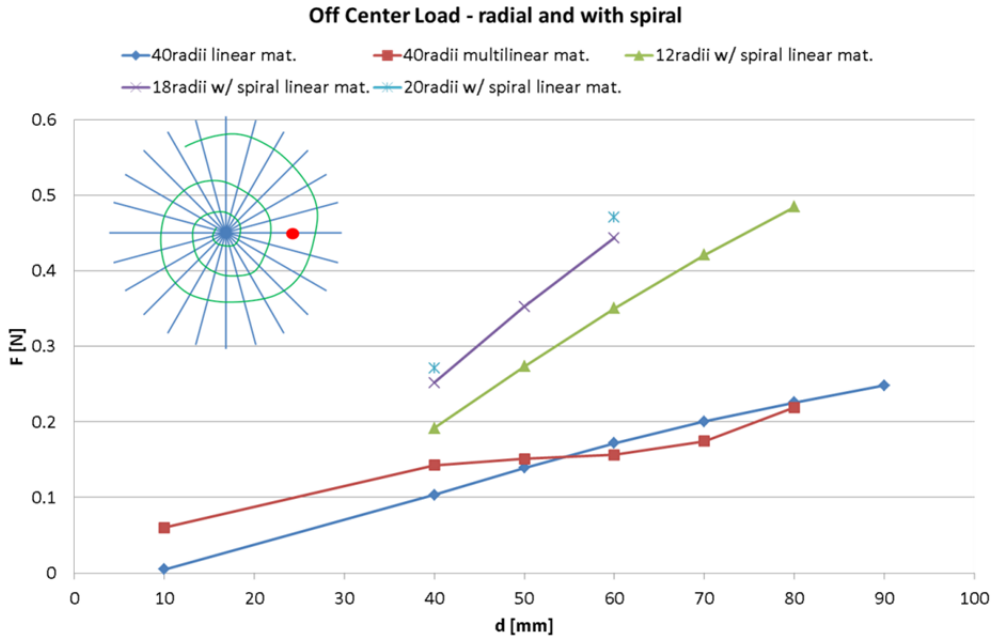

Figure 3-14 Off center load complete web. The curves are up to the first element break

From the results the stress concentration in a restricted area of the web is evident particularly when the load increases (Figure 3-15) as in the studies [11], [12]. As in the simple model the segment with the

higher stress is the shorter part of the loaded radius. The spiral transfers some stress to the nearest radii but the region with high stresses remain restricted to three radii. The general effect from the top view is a general translation in the direction of the application point.

3.1.6.1 Remarks

To increase the usability of the simulations a different model approach could be tried in order to reduce the solving problems found in the whole complex geometry simulations with the off center load and the spiral. Somehow a reduction of the elements' number is needed. (Table 3-4) reports the iteration parameters used to solve the off center cases with complete radii plus spiral. An improvement would be to find an approach to evaluate a priori the iterations needed for the nonlinear solution. The results with the spiral are only for the linear material model and it was not possible to solve the 40 radii structure with this material so knowing that when the multilinear material is introduced the solution is harder to find the effort was to first solve an easier problem, i.e. less radii. Even though the linear model and a reduced number of radii have been used an important characteristic appears: indeed with less material the structure has improved the load capacity. The volume is reduced because of the fewer radii that are the principal element in structure resistance to the charge but also since the greater γ also the spiral becomes in less dense, i.e. distance between turns increase, and require less material.

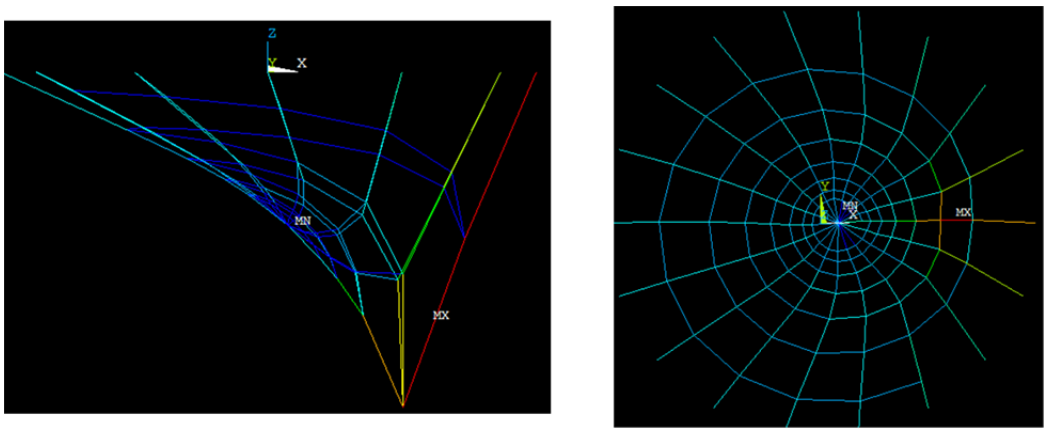

Figure 3-15 Example of FEM simulation results: the effect on the web of the off center load is a general translation to the right when observed from the top. The stress is localized in the sector near the displacement application point. Structures with 18 radii under a 40 mm displacement (on right) and 12 radii under a 50 mm displacement (on left).

Table 3-3 Force values at different displacements in web structures. X is broken structure.

	F [N] for linear material				
	off center	off center with spiral			center
d [mm]	40 radii	12 radii	18 radii	20 radii	40 radii
80	0.2259	0.4849	x	x	2.5801
70	0.2004	0.4210	x	x	2.1622
60	0.1717	0.3506	0.4439	0.4710	1.7577
50	0.1393	0.2736	0.3528	0.3738	0.8707
40	0.1031	0.1917	0.2520	0.2707	1.3054

Table 3-4 Solver parameters for the complete web structure in off center case.

	number of substeps and minimum iteration number		
d [mm]	12 radii	18 radii	20 radii
80	9e5/100	-	-
70	999999/50	5000000/500	-
60	999999/50	999999/500	8000000/200
50	9999/200	999999/500	3500000/200
40	9999/5	999999/200	100000/200

Chapter 4. Conclusions

The study led to the development of a procedure that can be applied again on new threads of different type and new configurations of the structure. From the testing procedure to the simulations' results all can be repeated with the same algorithms and generation codes. Thus now that a way has been chosen and a procedure developed it has to be improved the production, test more kind of fibers and improve aspects like impact tests or material combination.

The production aspect has to be deeply analyzed because fabrication is a not repeatable feature. The instability phenomenon complexity and also the lack of reliability under the point of view of the deposition parameters reproducibility led to obtain good results just a straight thread but at least the right choice of needle was made and should work for many different fibers' types.

The idea at the beginning of the project was to arrive at an impact test starting from the wire deposition knowledge which had been acquired previously. Here only the working results were reported but it could be useful tell a bit the history of how we get there. Over time the path that leads to this goal was discovered longer than thought but still, regardless the difficulties, we are about to make a first test on a complete web knowing the role of the structural components. At the beginning of this work the production was the focal aspect: the first attempt was with the $200\mu m$ needle as it had been studies before by [19]. Test attempts were done after finding the good set up: a first test was made on a smaller traction machine which had no sufficient crossbeam displacement range to break and develop all the loops. With the new equipment the results of the 200µm exhibit a not repeatable behavior. Straight lines were absolutely unreliable (Figure 4-1) and broke at negligible displacements, considering the initial length of about 2 cm and compared with the expectations. It was probably due to their irregular cross section not circular but flat and twisted in looped threads as can be seen in (Figure 1-10 on the right). The looped fibers had different behaviors some broke immediately but

others had quite a good result considering that certain bonds broke (Figure 4-2 and Figure 4-3).

The smaller 30 μm needle was used based on the previous experience of Frédérick Gosslein. This time the tests gave good results at least for the straight fibers, these are the results that were used here, but still the fibers with sacrificial bonds were not successful (Figure 4-4) because the link were too strong.

The implementation of the simulation codes was simultaneous to the production and preliminary cases were tested to verify the models with arbitrary material properties. Starting with these simulations, some with FE other analytical, gave some hints on how make the model and allowed to develop a critical knowledge. When the mechanical tests gave positive results, they were analyzed and included in the ready simulations. Thus the final result here reported appeared: when an external object is hanged on the web structure depending on where it is applied the geometry and material work differently:

- when the load is at the center the spiral has no influence thus the best geometry is a pure radial one; the multilinear material work better than the linear for small deflections.
- if the load is not perfectly centered the more it is on a side the more the spiral becomes important to reduce the deformation. Increasing the number of radii produce a stiffer structure even though the supported force is an order of magnitude smaller than in the central case.

The simulations studied a static situation but they can provide information also for dynamic cases like an impact: the simple evaluation of the work done by the force indicates approximately the magnitude of energy that the structure could be able to adsorb thus an approximate kinematic energy of the impact. To evaluate this work the deformation history has to be taken into account as it is the area under the force displacement curve.

The failures were always local indeed only the loaded radius broke and the rest of the structure was still intact and potentially able to resist another load. In these simulations the action was always applied targeted in a point on radial element instead in nature it is on a surface that covers both the radii and the spiral. This could be simulated with a nodes rigid coupling or with a plane element. The absorbed energy however is always related to the radii also in spider

webs, [11], which are made by two different silks instead of a single material like the models here.

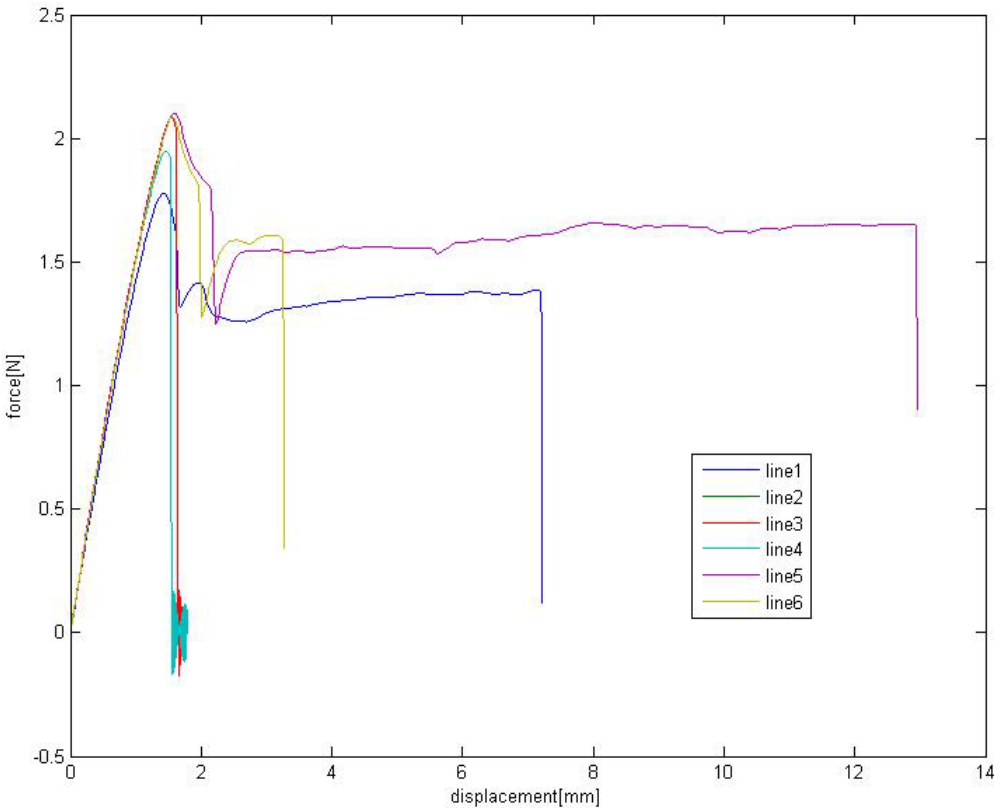

Figure 4-1200μm straight fiber tension test results.

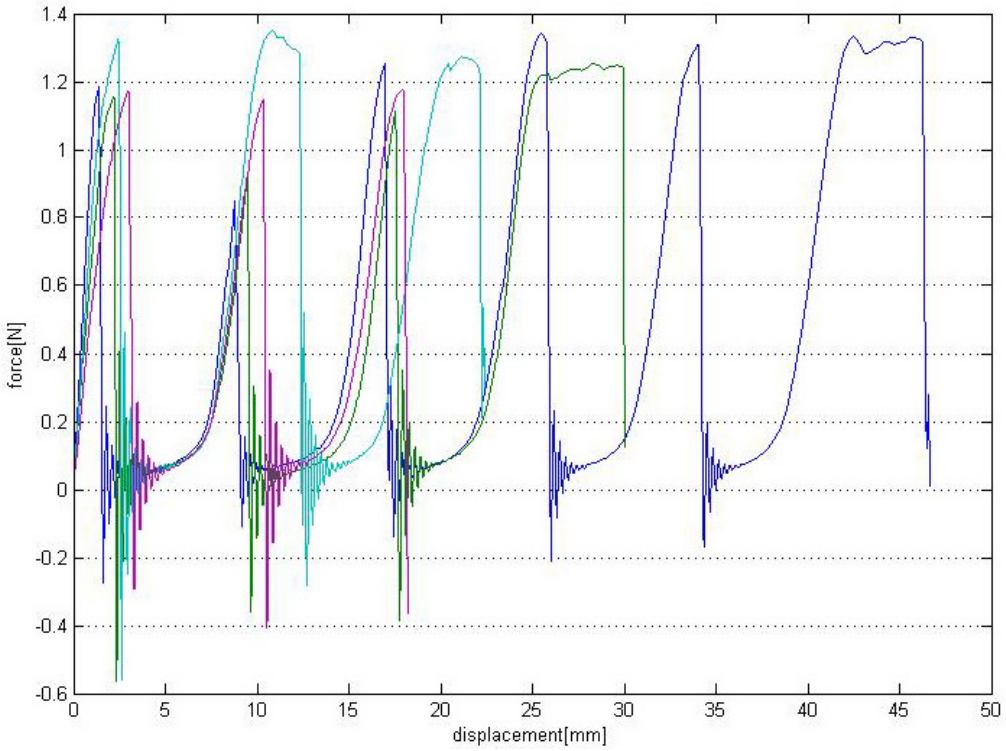

Figure 4-2 200 μm fibers with broken sacrificial bonds: they are not repetitive but demonstrate that the idea could work.

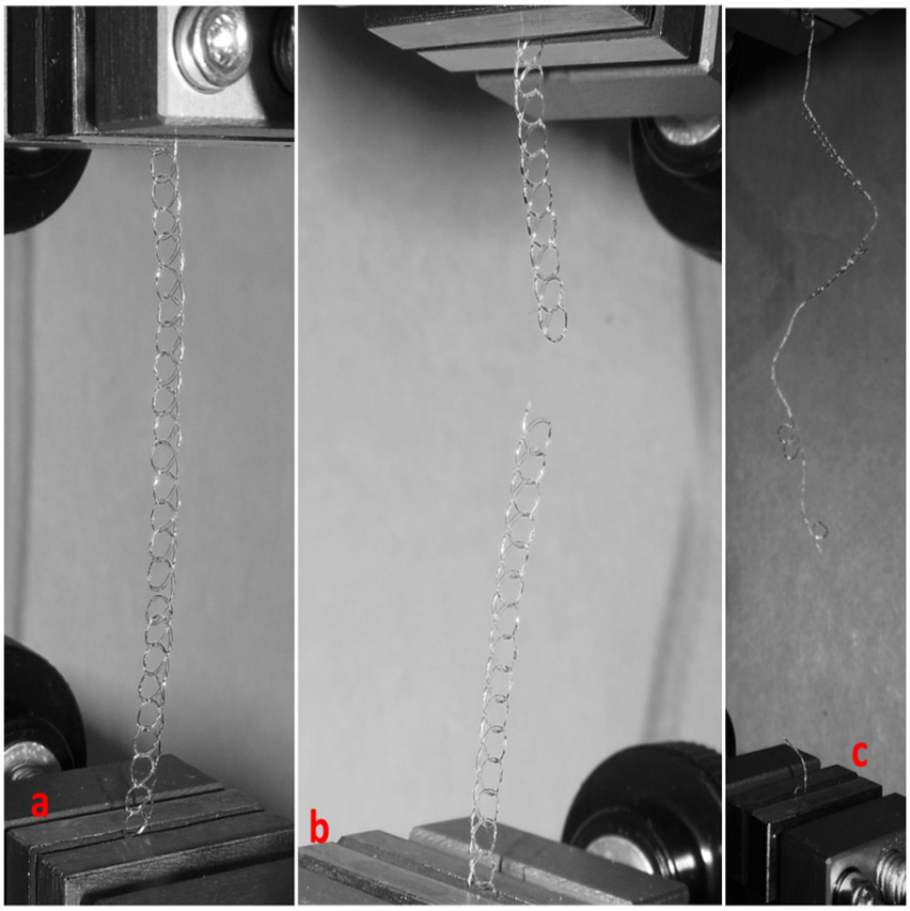

Figure 4-3 Typical condition for a 200 μm wire: a) before test, b) immediate failure and c) broken sacrificial bonds

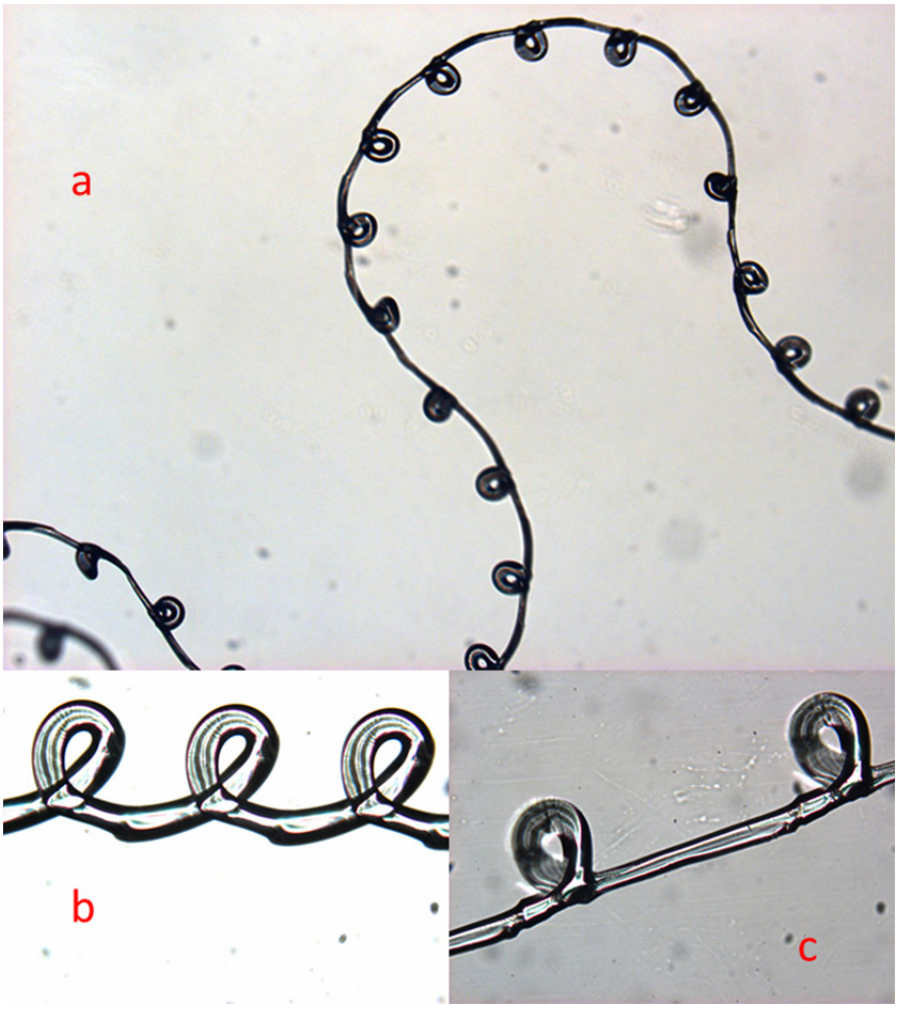

Figure 4-4 30 μm fibers with too strong bonds: the wire extension was only in between joints. (a) is a large view of this effect: a segment before (b) and after (c) the tension test.

Chapter 5. Future developments

In this section some advice for the future is given. They are divided into categories based on the main aspect of investigation.

5.1 Production improvement

A crucial aspect in this project was the threads production because it depends on many parameters: those that can be directly regulated by the operator and the external factors that have a greater influence the more the needle's diameter is small.

A good starting point is to improve the knowledge behind the production: this implies the study of solution's properties and their variation in time during the process and operation cycles. A work that is already in progress is the study of the DCM diffusion through the solution which should lead to the evaluation of the evolution of the solution during the deposition so at what time the solution conditions are better to create a sacrificial bond.

Another aspect is the fluid dynamics exiting the needle that could predict the theoretical diameter, taking account of the die swell effect, and the speed of the jet with the Ostwald model. It would aim to know the velocity rate with the substrate speed before production that characterizes the thread typology, straight, squiggly or looped. Maybe more complicated but for sure important is to develop a model of the instability (like in [[18]] but less complicated) to reach a good repeatability of loops geometry and the ability of its prediction.

Like it has been done for the 200µm in [19], a study of different parameters influence on the resulting fiber typology could be done also for the 30µm. Even though trying to create a map of the repeatable conditions function of parameters for the smaller scale could become complicated. In fact presently with a 30 µm needle it's necessary each time to recalibrate the deposition parameters because the result wouldn't be the same as expected if the operator just reapply the same set that was used before. This is due to external factors: the substrate not perfectly leveled, to the variability of the

needle's diameter and to the solution elements real ratio. Those factors can lead to a pressure modification of tens of KPa at the control unit to obtain a similar resulting thread. The same is less evident with a greater needle, like the 200μm. Moreover, they will have a great effect when the dimensions of the samples will increase to produce a web structure to test. The overlapping will modify the height and the deposition in many different directions will emphasize the possible imperfect level of the substrate in addition to the perturbation caused by curved trajectory or corners in the instability phenomenon. In the few attempts of creating a web structure made with a 200μm needle (see Figure 5-1) these problems caused a change in instability side and unlinked bonds at the end of the spiral, probably due to the long time required to ultimate the spiral. With a 30μm they will be critically important as those problems are already present in linear depositions (Figure 5-2).

5.2 Mechanical tests

All previous modifications have to be coupled with tests on any interesting type of thread. Other steps to do in this field are: out of plane static deformation tests, tension tests with high strain-rate and impact tests.

The perpendicular load test, both loads at the center and off center, is the direct application of FEM simulations; it can be done on a single wire at first as model validation. A possible set-up could be based on the TestResources grips and a series of masses to apply the load and increase it to follow the structure deformation. This way it would be also possible the control of the point of load application following its path obtained for different forces so to have data on breaking value and evolution for each fiber to compare with the simulation result. Then the tests on the radial structure would be done with two drilled plexiglass plates that guarantee the grip thanks to a rubber surface and a set of screws.

The tension tests with higher strain rate are necessary to verify the behavior under a rapid load application as in (Figure 1-4) because it will be different due to the viscoelastic characteristics of the PLA. This could be done as uniaxial tension test on the MTS Insight system and with the acquired experience of the statics cases adapted to the out of plane load situation in the FE models. Or it could be chosen to go directly for the perpendicular tests on a single fiber. The latter solution would mean a backwards path to calculate the single

wire properties and use the FE but it should save one iteration step for the easier model validation.

The final point would be the impact test which would complete the research and lead to a work of improvements under the material aspect, maybe with composites threads, or with new configurations like a fabric. A possible organization of the fibers to create a woven structure would be 0/90/±45 as angles of direction (Figure 5-4) thus to have a series of crossing strands like in a pure radial structure with $\gamma = 45°$ *or* $90°$ that covers the surface.

Figure 5-1 A 18 cm diameter web structure deposition attempt, made with a 200µm needle.

Figure 5-2 Instability inversion in two 30μm depositions.

5.3 FEM enhancement

Following the methodology explained in this study different aspects could be deeper analyzed or enhanced in the codes. Following the material evolution and tests results, different models could be integrated in the simulations: both using one single material for the whole structure and studying the combination of different materials for the radii and the spiral. Also the geometry should be tested developing new ones: the Bernoulli spiral does not look appropriate but the arithmetic, or Archimedean, spiral is the one that spiders use. Other geometries like simple circles instead of a spiral should be investigated as also adding some circle to the actual structure to see if it would increase the off center rigidity reducing so the load difference between center and off center cases.

Keeping the actual geometry, or new ones, a study on the material distribution could be done. If the total volume is limited and fixed, like in the syringe for the deposition and in spider body, the material could be allocated in different proportion between the radii and the spiral. On this subject some preliminary experiences have already been done. Starting from a pure radial structure and reducing the radii cross section, to obtain sufficient volume, a spiral was created each time with greater section. As predictable the structure transversal deformation increased always because the principal structural elements, the radii, were getting thinner. The same Matlab volume code could be used to repeat the experience this time reducing the number of radii, instead of their section which is not practically possible because it means change the needle so find new deposition parameters, and using their volume to add spiral segments, maybe not a whole spiral. A clue is in the off center load results where the

number of radii and the spiral length was progressively increased obtaining more resisting structures with more material so there could be an optimum repartition.

Under the computational aspect beyond the number of substeps for the solver, the reading of results could be computerized adding a saving component to the input code thus to have all the data in a output file, a text file, so the user does not need to read them manually each time but with a script different output can be compared at once. A great improvement would be to discover how to run several simulations one after the other directly from the input file. This would allow to make studies like material volume distribution faster or simulations of different displacement without opening any single file manually To reduce the elements' number an idea could be to create all the radii as single elements with multiple partitions for the spiral intersections. This would reduce the keypoints and create a geometry on which other elements are applied, with other FEM software is possible but the fact of having a major geometry could create some limitations for the internal partition deformation, for example if a straight line is the main geometry it has to curve due to internal partition.

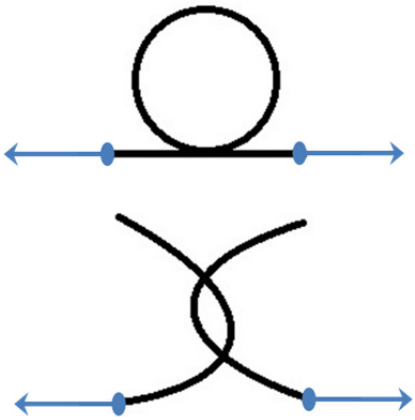

Figure 5-3 Possible geometries for sacrificial bonds strength test.

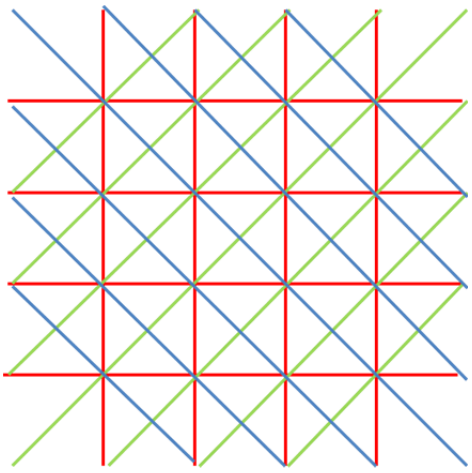

Figure 5-4 Wires orientation: red 0 and 90, blue -45, green +45 degrees.

5.4 Failed tests

Together with a better theoretical comprehension an experimental study could be done on the strength of the sacrificial bonds. It could proceed in parallel with the study of parameters suggested in 5.1 or it could be developed aside with a simple circular geometry or other overlap geometry to test (examples in Figure 5-3). At first this geometries could simply be drawn giving the whole coordinates to the robot, instead of using the filament instability to create overlapping. This is an easier step even though the high instability frequency for 30μm needle is difficult to draw. It would lead to find the optimal conditions for a good connection that is neither too stiff nor too weak. This in addition to diffusion time should give a very good knowledge on sacrificial bonds production. One way or the other the junction has to be characterized as function of time, instability frequency, i.e. height of deposition, pressure and relative speed.

It is important to find the right parameters for the bonding because tests have been done without appreciable results both for 30μm and 200μm needle deposited fibers. As shown the wires' backbone broke in first place or after just few bonds have been broken, when the bonds were correctly formed. Best results were encouraging, even though few loops were broken, producing a curve as expected. In other cases, when the connections were only overlaps without really be linked they simply unrolled and the wire acted like a spring. To reduce the bonding strength in those cases where the wire broke before every bond a lower pressure or a greater height should be used and vice versa for the non-linked cases.

Bibliography

[1] M. Denny, "The physical properties of spider's silk and their role in the design of orb-webs," *exp. Biol.,* no. 65, pp. 483-506, 1976.

[2] F. Vollrath, W. Mohren, "Spiral Geometry in the Garden Spider's Orb Web," *Naturwissenschaften, Springer-Verlag,* no. 72, 1985.

[3] Fritz Vollrath, Mike Downes, Sven Krackow, "Design Variability in Web Geometry of an Orb-Weaving Spider," *Physiology & Behavior,* vol. 62, no. 4, pp. 735-743, 1997.

[4] M. E. Herberstein, A. M. Heiling, "Asymmetry in spider orb webs: a result of physical constraints?," *Animal Behaviour,* no. 58, pp. 1241-1246, 1999.

[5] Eckhard Wirth, Friedrich G. Barth, "Forces in the spider orb web," *Journal of comparative physiolgy A,* vol. 171, pp. 359-371, 1992.

[6] V. Fritz, "strength and structure of spiders' silks," *Molecular Biotechnology,* no. 74, pp. 67-83, 2000.

[7] Fritz Vollrath, Bo Madsen , Zhengzhong Shao, "The effect of spinning conditions on the mechanics of a spider's dragline silk," *Proc. R. Soc. Lond. B,* vol. 268, no. 1489, pp. 2339-2346, 2001.

[8] Xin Chen, Zhengzhong Shao and Fritz Vollrath, "The spinning processes for spider silk," *Soft Matter, The Royal Society ot Chemistry,* no. 2, pp. 448-451, 2006.

[9] J. M. Gosline, P. A. Guerette, C. S. Ortlepp, K. N. Savage, "The mechanical design of spider silks: from fibroin sequence to mechanical function," *The Journal of Experimental Biology,* no. 202, p. 3295–3303, 1999.

[10] John M. Gosline, M. Edwin DeMont, and Mark W. Denny, "The structure and properties of spider silk," *Endeavour,* vol. 10, no. 1, pp. 37-43, 1986.

[11] Andrew T. Sensenig, Kimberly A. Lorentz, Sean P. Kelly and Todd A. Blackledge, "Spider orb webs rely on radial threads to absorb prey kinetic energy," *J. R. Soc. Interface,* 2012.

[12] Steven W. Cranford, Anna Tarakanova, Nicola M. Pugno & Markus J. Buehler, "Nonlinear material behaviour of spider silk yields robust webs," *Nature,* vol. 482, 2012.

[13] Fritz Vollrath, David P. Knight, "Liquid crystalline spinning of spider silk," *NATURE,* vol. 410, 2001.

[14] Georg E. Fantner et Al., "Sacrificial Bonds and Hidden Length: Unraveling Molecular Mesostructures in Tough Materials," *Biophysical Journal,* vol. 90, pp. 1411-1418, 2006.

[15] Nathan Becker Et Al., "Molecular nanosprings in spider capture-silk threads," *Nature,* vol. 2, 2003.

[16] Georg E. Fantner Et Al., "Sacrificial bonds and hidden length dissipate energy as mineralized fibrils separate during bone fracture," *nature materials,* vol. 4, 2005.

[17] A. Volkwein et Al., "Rockfall characterisation and structural protection – a review," *Nat. Hazards Earth Syst. Sci.,* no. 11, pp. 2617-2651, 2011.

[18] M. Pierre-Thomas Brun, Dynamique des filaments élastiques et visqueux, Thèse de doctorat de l'université Pierre et Marie Curie, 2012.

[19] A. Faure, "Synthèse fibreuse par instabilité du cordon fluide: Cartographie et étude expérimentale pour le mélange PLA/DCM," Ecole Polytechnique De Montreal, 2012.

[20] ASTM D3822-07, *Standard Test Method for Tensile Properties of Single Textile Fibers.*

List of figures

List of tables